九州大学学術情報リポジトリ
Kyushu University Institutional Repository

Study on Output Current Behavior of Electrochemical Apparatus Sensitive to Antielectron Neutrinos

ヌール, アイダ

https://doi.org/10.15017/1398349

出版情報：九州大学, 2013, 博士（工学）, 課程博士
バージョン：
権利関係：全文ファイル公表済

Study on Output Current Behavior of Electrochemical Apparatus Sensitive to Antielectron Neutrinos

NUR AIDA

Doctoral Dissertation

Study on Output Current Behavior of Electrochemical Apparatus Sensitive to Antielectron Neutrinos

By

NUR AIDA

Department of Applied Quantum Physics and Nuclear Engineering
Graduate School of Engineering, Kyushu University, Japan
July 2013

Contents

Chapter 1 Introduction

1.1 Neutrino History

A neutrino is one of fundamental particles in the universe. It is a neutral particle without electric charge, and has a very small mass. Neutrinos are very difficult to detect because they are not affected by electromagnetic forces, only with gravity and weak interaction. There are three types of neutrinos; electron neutrinos, muon neutrinos and tau neutrinos, respectively. Each type is associated with antineutrino as an identical particle but opposite in helicity. The Neutrino was first postulated by Wolfgang Pauli in 1930[1], after confusing with the beta-decay phenomena. Beta-decay seems violate from the law of energy conservation. In beta-decay, a neutron transforms into a proton and electron and followed with the continuous spectrum[2] . The continuous beta spectrum was quite different from a discrete alpha and gamma spectrum. It was surprising many physicists and become interested topic at the time. Neils Bohr proposed a statistical method of conservation law to explain the phenomenon[3]. He suggested that energy may only be conserved on 'averaged', however, Compton effect provided different suggestion on this view.

In 1930, Wolf Gang Pauli wrote a letter to Hans Geiger and Lisa Meitner[1], to define that a misunderstanding light of beta spectrum is an uncharged particle, this particle could carry the missing energy, undetected, and emitted together with the electron. Pauli hypothesis provides the balancing of the energy conservation by the reaction,

$$n^0 \rightarrow p^+ + e^- + \bar{\nu}_e \tag{1.1}$$

He defined an undetected particle as 'neutron'. However, James Chadwick discovered a massive nuclear particle also named neutron. In 1933, Enrico Fermi, changed the name of uncharged particle into neutrino which means 'little neutral one' to distinguish it between neutron[4] . After it postulated, many physicists concern about neutrinos for many years. Fermi submitted the theory of beta decay with an idea of

neutrino to an Italian Journal, after rejected from the journal Nature, and it was served as a theoretical principle for the neutrino experiments.

In 1942, Kan-Chang Wang first proposed experimental detection of neutrinos by using beta capture[5]. In 1956, Clyde Cowan and Frederick Reines, confirmed that they had detected the neutrino by the antineutrino experiments[6], and Reines received a Nobel Prize of this result after forty years later. Their experiment was conducted in a nuclear reactor where antineutrinos were formed of beta decay. the neutrino then reacted with protons and producing neutrons and positrons by reaction:

$$\bar{\nu}_e + p^+ \rightarrow n^0 + e^+ \tag{1.2}$$

The positron easily combined with electron then annihilated each other and emitting two gamma rays (γ) as the result. The neutron can be detected by its capture on a nucleus, releasing a gamma ray. These two events, tend to a clearly evidence of the antineutrino interaction. In 1962, Leon M. Lederman, et.al., first detecting the interaction of muon neutrino from the decay chain of $\pi^+ \rightarrow \mu^+ \rightarrow e^+$. It was assumed that a neutrino is emitted in the opposite direction to the muon (μ^+), the neutrino originated from muon reaction was definitely different behavior with the neutrino of electron decay[7]. This experiment earned them to the Nobel Prize in 1998.

The third type of neutrino was first observed at the Stanford Linear Accelerator Center, as in beta-decay, the missing energy and momentum of tau decays suggested to discover a tau neutrino[8]. The first detection of tau neutrino interaction was announced by the DONUT collaboration at Fermilab in July 2000, and its exsistence had already proven by theoretical and experimental data. Neutrinos are belongs to the family of leptons. Three types of neutrinos also called three flavors are completing their existence[9]. Each flavor are associated with the charge of particle in the Standard Model of particle physics, and were namely in related to the reaction of particle from they were discovered, as electron neutrino, muon neutrino and tau neutrino, it is indicated in **Table 1.1**.

Antineutrinos are the antiparticles of neutrinos, which are also neutral particles produced during beta particle emissions, and have a spin of $\hbar/2$. The antineutrinos all have right-handed helicity, while the neutrinos are left-handed. Mass of neutrino

was considered zero until the neutrino oscillation experiments observed that neutrinos constitute of mass between 0.05 and 8.4 eV/c^2[11]. Because antineutrinos and neutrinos are neutral particle, it was considered that they are actually the same particles. Particles with this property are known as Majorana particles[10]. Antineutrinos were first detected as a result of their interaction with protons in a large tank of water. This was installed next to a nuclear reactor as a controllable source of the antineutrinos[11].

Table 1.1 The three generations of leptons and their associated neutrinos in the Standard Model of particle physics.

Generation	Lepton	Neutrino
First	Electron, e^- Positron, e^+	Electron neutrino, v_e Electron antineutrino, $\bar{v}_e$
Second	Muon, μ^- Antimuon, μ^+	Muon neutrino, v_μ Muon antineutrino, $\bar{v}_\mu$
Third	Tau, τ^- Antitau, τ^+	Tau neutrino, v_τ Tau antineutrino, $\bar{v}_\tau$

1.2 Sources of Neutrinos

The universe is consisted of neutrinos which are produced from physical processes or exist naturally. Neutrinos play an essential factor in the violent processes such as Big Bang and radioactive decay observed on the earth. Eventhough neutrinos pass our body everyday, as a neutral particle they will not affect the matter. The existence neutrinos are considered originated from the sources as follow.

1.2.1 Nuclear Reactors and Accelerators

Nuclear reactors and particle accelerators are the source of artificial neutrinos[12]. Generally, the four main isotopes, ^{235}U, ^{238}U, ^{239}Pu and ^{241}Pu, generate electron antineutrinos ($\bar{\nu}_e$) flux through beta-decays in the fuel. The reactions are given in **Fig. 1.1**. It is well understood that when a ^{235}U nucleus captures a neutron, it will be transformed into an excited state of ^{236}U* which produces two fission fragments and neutrons. As well as electron antineutrinos are generated with beta rays and gamma rays during the fission process. ^{238}U nucleus absorbs a neutron to create ^{239}U that mostly changes into ^{239}Pu through the beta decay. ^{239}Pu captures neutrons to form ^{241}Pu, ^{238}U, ^{239}Pu. The electron antineutrinos are generated from ^{241}Pu through beta decay.

$$^{235}_{92}U + n \rightarrow {}^{236}_{92}U^{*} \rightarrow \text{ ff1 + ff2 + n}$$

$$\downarrow \text{ Decay of ff1 and ff2}$$

$$\beta^{-} + \bar{\nu}_e$$

$$^{238}_{92}U + n \rightarrow {}^{239}_{92}U + \gamma \qquad {}^{239}_{92}U \rightarrow {}^{239}_{93}Np + e + \bar{\nu}_e\,, \qquad {}^{239}_{93}Np \rightarrow {}^{239}_{93}Pu + e + \bar{\nu}_e$$

$$^{239}_{94}Pu + n \rightarrow {}^{240}_{94}Pu + \gamma\,, \qquad {}^{240}_{94}Pu \rightarrow {}^{241}_{94}Pu + \gamma\,, \qquad {}^{241}_{94}Pu \rightarrow {}^{241}_{95}Am + e + \bar{\nu}_e$$

$$^{242}_{94}Pu + n \rightarrow {}^{243}_{94}Pu + \gamma\,, \qquad {}^{243}_{94}Pu \rightarrow {}^{243}_{95}Am + n + \bar{\nu}_e$$

Figure 1.1 The fission reaction of ^{235}U, ^{238}U, ^{239}Pu and ^{241}Pu isotopes for generation the electron antineutrinos in the reactor core. ff1, ff2 are the fission fragments.

The energy about 200 MeV in average releases from nuclear fission, and roughly 4,5% (about 9 MeV) is radiated away as antineutrinos. Such as nuclear reactor with a thermal power of 4000 MW, and electrical power of 1300 MW, the total power should be 4185 MW, about 185 MW is radiated away as antineutrino radiation and lost in the process. That means 185 MW of fission energy does not appear as the presence heat to turn turbine, the antineutrinos can penetrate the reactor building without any trace and undetectable.

The energy spectrum of anti neutrinos depend on the fuel materials, for example, the antineutrinos energy spectrum from plutonium-239 fission are more slightly than

those from uranium-235 fision. However, the detected antineutrinos from fission have a peak energy range about 3.5 - 4 MeV, with a maximum of about 10 MeV. Until now, no experiments established the procedure to obtain the flux of low energy anti neutrinos, the only identified is antineutrinos with an energy above threshold of 1.8 MeV. About 3 % of all antineutrinos from a nuclear reactor carry energy above this threshold. A typical nuclear power plant may generate antineutrinos above 10^{20} per second above this threshold and also produce a much larger of energy below the threshold still cannot be seen with the present detector technology.

The particle accelerators have been used to make neutrino beams, by injecting protons into a fixed target, and produce pions or kaons. In the case of Los Alamos Neutron Science Center (LANSCE), the linear accelerator[13] uses conventional ion sources for protons. Ion sources provide particles for acceleration that are selected on a pulse - by - pulse basis. Protons passed through a transition section to a drift tube linear accelerator. Protons are accelerated in this section and then injected directly into a side coupled linac structure for acceleration to a nominal energy of 800 MeV. When a proton beam (<1 GeV) is stopped by a thick target[14], about 10% of the interacting protons produce pions via the reaction a quarter of the positive pions (π^+) are absorbed, while those remaining stop and decay to produce equal numbers of muon neutrinos (v_μ) , muon antineutrinos ($\bar{v}_\mu$), and electron neutrinos (v_e) :

$$p + target \rightarrow \pi^{\pm} + X, \tag{1.3}$$

$$\pi^{\pm} \rightarrow \mu^{\pm} + v_\mu(\bar{v}_\mu),$$

$$\mu^{\pm} \rightarrow e^{\pm} + v_\mu(\bar{v}_\mu) + v_e(\bar{v}_e)$$

Because the producing neutrinos close to the protons beams than isotropically, efforts to constuct an accelerator facility where the neutrino are produced through muon decays are ongoing[15]. It is known as a neutrino factory. Nuclear bombs also produce very large quantities of neutrinos. Fred Reinesand Clyde Cowan considered the detection of neutrinos from a bomb prior to their search for reactor neutrino[16].

1.2.2 Geoneutrinos

The earth has kept many radioactive atomic nuclei since its birth. Neutrinos are part of the natural background radiation. In particular, the decay chains of ^{238}U and ^{232}Th isotopes, as well as ^{40}K, include beta decays which emit antineutrinos. These so-called geoneutrinos can provide valuable information on the earth's interior. Particularly, related to the angle dependent measurement of the geoneutrinos flux could help to indicate the areas with a high radioisotope content[12]. A first indication for geoneutrinos was found by the kamLAND experiments in 2005[12]. The main background on this experiments are the antineutrinos coming from reactors. Several future experiments aim to improving the geoneutrinos experiment and these will be necessary to be far away from reactors.

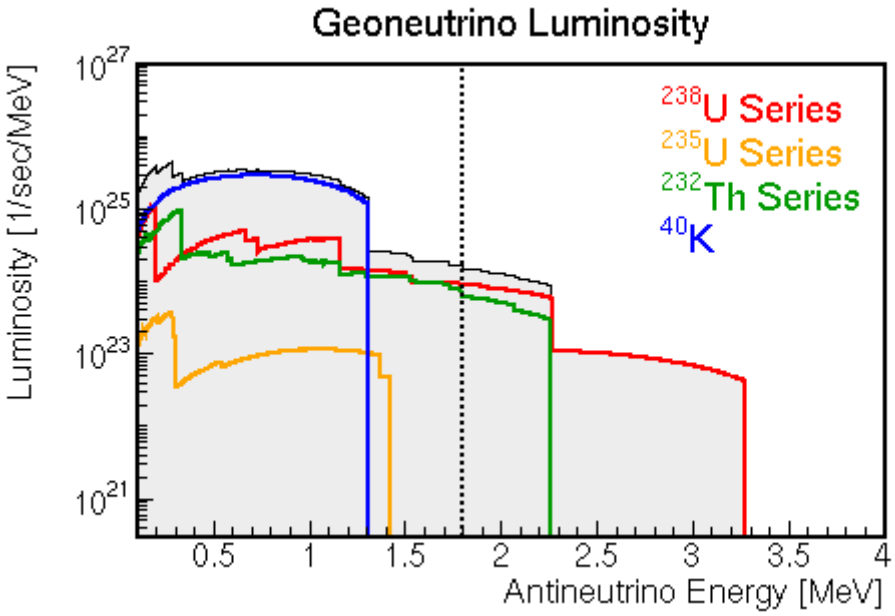

Figure 1.2 Energy spectrum of geoneutrinos. The vertical dotted line indicates the detection threshold at 1.8 MeV

1.2.3 Atmospheric Neutrinos

Atmospheric neutrinos are produced in the earth's atmosphere from the interaction of cosmic rays with atomic nuclei. The cosmics rays are consist of 89% of protons,

10% of helium, and 1% of heavier element nuclei. At the energies up to 10^9 eV, the cosmic rays go into the upper atmosphere, and collide with atoms. The collision process emits a wide quantity of secondary particles including pions which are fell down to the earth's surface. The pion directly decays to a muon and a muon-type neutrino, the muon in the turn decays to an electron, electron-type neutrino, and a muon-type neutrino. These processes are explain by eqs. (1.4) and (1.5).

$$p \rightarrow X + \pi^+, \quad \pi^+ \rightarrow \mu^+ + \nu_\mu, \quad \mu^+ \rightarrow e^+ + \nu_e + \bar{\nu}_\mu, \tag{1.4}$$

$$p \rightarrow X + \pi^-, \quad \pi^- \rightarrow \mu^- + \bar{\nu}_\mu, \quad \mu^- \rightarrow e^- + \bar{\nu}_e + \nu_\mu, \tag{1.5}$$

Through the decay of pions and muons, high energy muon-type and electron-type neutrinos are produced in the ratio of 2:1.

1.2.4 Solar Neutrinos

Solar neutrinos are originated from fussion reaction of the sun and other stars. The Standard Solar Model (SSM) explains more about the operation process inside the sun[19]. Shortly, when four protons fuse to make one helium nucleus, two of them will convert into neutrons, and each conversion releases one electron neutrino by the reaction [20].

$$4p \rightarrow {}^4He + 2e^+ + 2\nu_e + \gamma, \tag{1.6}$$

Generally neutrinos are occur via two main chains reaction, Most of neutrinos (98.4%) are produced by the proton – proton (pp) chain, while the rest (1.6%) are emitted from the carbon – nitrogen – oxygen cycle (CNO) chain. The chains are shown in **Figs. 1.3** and **1.4**. The pp chain produces five reactions of neutrino sources, its three sources produce continuum neutrino spectra, namely, pp neutrinos, hep neutrinos, and the ^{8}B neutrinos. The pp and ^{8}B are familiar sources of neutrinos. There are also two sources of pp neutrinos with discrete energies: the pep and ^{7}Be neutrinos.

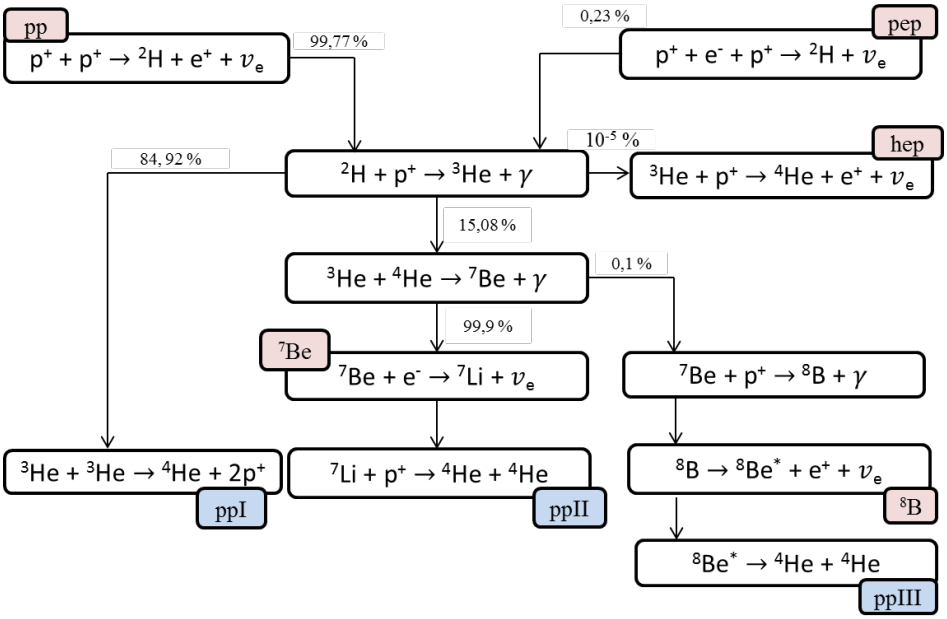

Figure 1.3 Proton-proton chain reactions in the sun

The ^{13}N, ^{15}O and ^{17}F reactions contribute three neutrino sources as CNO cycle. The ^{17}F is the most potential one, since its flux produces oxygen in a large quantity in the sun.

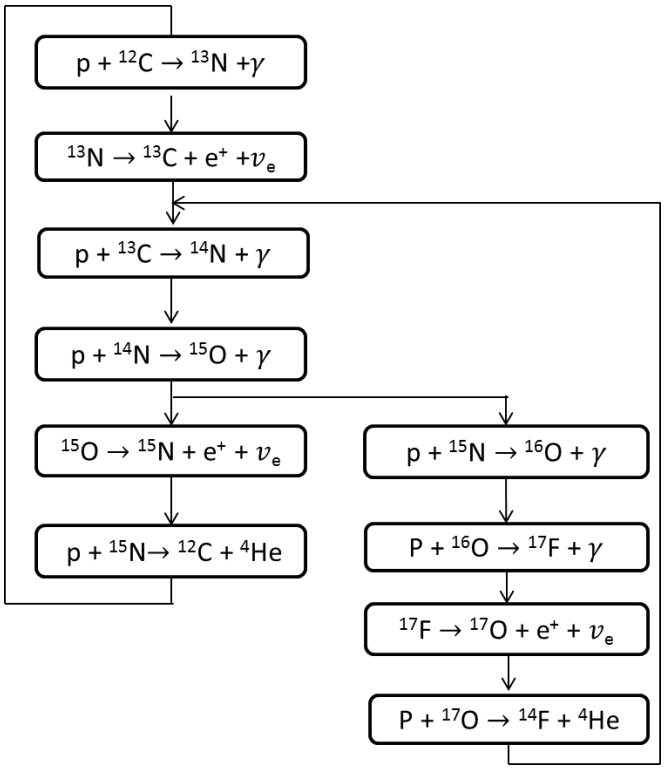

Figure 1.4 Carbon-nitrogen-oxygen chain reactions in the sun

Figures. 1.3 and 1.4 give the reactions of particle in Standard Solar Model. In contrast to the pp-chains, the CNO cycle only provides a small contribution of solar neutrino generation. It is related to the temperature in which the solar neutrinos are generated[21], the solar neutrino flux depends on the solar core temperature. ^{8}B neutrinos are produced at the highest temperature following to ^{7}Be neutrinos.

The Sun sends enormous numbers of neutrinos in all directions. Each second, about 65 billion (6.5×10^{10}) solar neutrinos pass through every square centimeter on the part of the Earth that faces the Sun[22]. Since neutrinos are difficult absorbed by the mass of the Earth, the surface area on the side of the Earth opposite the Sun receives about the same number of neutrinos as the side facing the sun.

1.2.5 Supernovae Neutrinos

Supernova neutrinos was first observed by Colgate and White in 1966[23], they hypothesized that neutrinos carry away most of the gravitational energy which is exist from the collapse of massive stars, when a massive star depletes its supply of nuclear fuel, it collapses and density of matters at the core becomes so high (10^{17} kg/m^3), hence the degeneracy of electrons is not enough to protect the combination of proton and electron to form a neutron and electron neutrino. The process is called electron capture. It can be written as.

$$e^- + p \rightarrow n + \nu_e \tag{1.7}$$

A second source is the thermal energy (100 billion kelvins) of the newly formed neutron core, which is dissipated via the formation of neutrino-antineutrino pairs of all flavors. [24] Colgate theory was confirmed in 1987, which detected the neutrinos from supernova by using two Water-based detectors, Kamiokande II and IMB [25]. While the scintillator based Baksan detector found 5 neutrinos originated of either thermal or electron capture, less than 13 seconds after explosion. The neutrino signal arrived to the earth several hours early than electromagnetic radiation. Since neutrinos have a feeble interaction with normal matter, it was allowed them to pass the star explosion easily while electromagnetic photons were slowed. The exact time delay depends on

the velocity of the shock wave and the thickness of the outer layer of the star. Neutrinos may carry information about the innermost region of the explosion. Many radioactive elements are formed by the supernova shock wave, and even light from the explosion itself is scattered by dense and turbulent gases. Neutrinos go by the explosion, providing the information about the supernova core.

1.2.6 Supernova Remnants Neutrinos

The supernova neutrinos have an energy range in tens of MeV. They are originated from the residual of turbulent gaseous environments of supernova explosions. It produces neutrinos at least one million times more energetic. The energetic neutrinos occur from supernova remnant was refined by Vitaly L. Ginzburg and Sergei I. Syrovatsky. Their hypothesis is suggested by the specific mechanism of 'shock wave acceleration' happening in supernova remnants, which received support from observational data from Baikal, AMANDA, IceCube. The very high energy neutrinos are to be seen, but this astronomy neutrino is just in its infancy.

Beside the neutrinos, the collisions of cosmic rays are also supposed to produce charged and neutral pions, the charged pions decay giving neutrinos, and neutral pions decay emitting gamma rays. Both types of radiations were evidence in a supernova remnant, these information were provided by very high energy gamma ray observatories, such as VERITAS, HESS and MAGIC. The higher energy neutrinos, resulting from the interactions of extragalactic cosmic rays, also observed by Pierre Auger Observatory with its experiment named ANITA.

1.2.7 Big Bang

The universe consists of elementary particle including neutrinos. Their balancing are reached by a thermal equilibrium. In the early universe with a temperature is more than 10^{10}K, the matter still in highly density and neutrinos are remained in equilibrium with others through the weak interactions. After 1 second of the Big Bang the universe

extremely cool. Thus, neutrinos decoupled from the rest of the matter before photons, and cooled strictly due to expansion of the universe.

The existence of dark matter in the universe is proposed in the 1980s, and neutrinos are also considered as one of dark matter candidates. Since neutrinos easily move at speeds close to the speed of light, the dark matter originated from neutrinos is termed as 'hot dark matter'. Neutrino's speed created them to spread out evenly in the universe before cosmological expansion. It is caused the contribution of neutrinos are not essential in the dark matter assumption.

From the cosmological sides, relic background neutrinos are estimated to have density of 56 of each type per cubic centimeter[26] and the present temperature of neutrinos from the Big Bang is expected to be 1.9K, if their mass exceeds 0.001 eV. The low neutrino cross-sections at sub-eV energies, caused their density to become quite high. The relic neutrino background has not yet been observed in the laboratory.

1.3 Neutrino Experiments

Neutrinos cannot be detected immediately because they do not carry electric charge, hence they do not ionize the materials they are passing through. Reines and Cowan found a unique reaction to observe antineutrinos by the inverse beta decay, their experiment requires a very large detector in order to detect a significant number of neutrinos. The neutrinos detection methods supposed neutrinos to have minimum threshold energy. So far, there is no detector applied to measure the low energy neutrinos, in the sense that potential neutrino interactions cannot be specifically distinguished from other causes. The neutrino detectors are often built underground to protect the detector from cosmic rays and other background radiation. The main experiments on solar neutrinos detection are explained below.

1.3.1 Borexino Experiment

Borexino is a particle physics experiment which observed low energy (sub-MeV) solar neutrinos. It Located at the Laboratori Nazionali del Gran Sasso Italy [27]. The goals of this experiment are measurement of solar neutrino flux from beryllium-7,

boron-8, pp, and pep. This experiment also concern on geoneutrinos and antineutrino from nuclear power plants. The detector is a high-purity liquid scintillator calorimeter, placed within a stainless steel sphere and shielded by a water tank. In 2011, it published a precision measurement of the beryllium-7 neutrino flux, [28] [29] as well as the first evidence for the pep solar neutrinos. [30] [31] In 2012, it published the results of measurements of the speed of CERN Neutrinos to Gran Sasso , where neutrinos speed were consistent with the speed of light[14].

1.3.2 Gallium experiment

Gallium Experiment[32] is a radiochemical neutrino detection conducted between 1991 and 1997 at the Laboratori Nazionali del Gran Sasso (LNGS). It detected low energy of solar neutrinos. The experiment components, is placed under 3200 metres in depth to shield it from cosmic rays. The detector tank (54-m^3) is filled with 30.3 tons of gallium acted as the target for a neutrino-induced nuclear reaction, which transmuted it into germanium.

$$v_e + {}^{71}Ga \rightarrow {}^{71}Ge + e^- \tag{1.8}$$

The threshold for neutrino detection by this reaction is 233.2 keV, This reaction is also able to detect neutrinos from the initial proton fusion reaction of the proton-proton chain reaction, with an upper energy limit of 420 keV. The solar neutrino flux measured by the GALLEX experiment is 77.5 SNU (Solar neutrino units), roughly 0.75 decays a day.

1.3.3 Homestake Experiment

In the 1960s, Bahcall and Davis calculated and collected the neutrinos emitted from nuclear fusion in the sun. The experiment was taken place in the Homestake Gold Mine in Lead, South Dakota. David set down 100,000 gallon of perchloroethylene, a common dry-cleaning fluid, in underground (1,478 meters) in depth. The target of this experiment is to account the very small probability of a successful neutrino capture, and to prevent interference from other forms of solar

radiation. Perchloroethylene was chosen because it contains chlorine. If a chlorine atom collides with a neutrino, it transforms into an argon isotope, with the threshold energy of 0.814 MeV release from this reaction. The argon atom then Be extracted and counted. Davis bubbled helium through the tank to collect the argon every week, and this process was able to determine how many neutrinos had been captured[33] [34].

$$v_e + {}^{37}Cl \rightarrow e^- + {}^{37}Ar \tag{1.9}$$

Davis's figures agreed with one-third of Bahcall's calculations. The Homestake experiment was followed by other experiments with the same purpose, Davis won the 2002 Nobel Prize in Physics. The rate of solar neutrino capture in solar experiment is usually expressed in SNU (Solar Neutrino Units, 1 SNU corresponds to 1 capture/s from 10^{36} nuclei). The results of Homestake experiment is[35] 2.56 $\pm$0.23 SNU.

1.3.4 Kamiokande

This experiment is placed under Mount Kamioka, Gifu Prefecture, Japan. The detector is built to catch proton decay of solar and atmospheric neutrinos. Super Kamiokande detector was designed with a large volume of water surrounded by photomultiplier tubes. The tubes were used as an imaging cerenkov counter. A neutrino interaction with the electrons could produce a charged particle that moves faster than the speed of light in water. It creates a cone of light known as Cherenkov radiation. The Kamiokande experiment is the first observation detected solar neutrinos by using the elastic scattering reaction

$$v + e^- \rightarrow v + e^- \tag{1.10}$$

The solar neutrinos flux attained by this reaction is [36] 2.32 x 10^6 $cm^{-2}s^{-1}$ at threshold energy of 5 MeV

1.3.5 KAMLAND

The Kamioka Liquid Scintillator Antineutrino Detector (KamLAND) is an experiment placed at the Kamioka Observatory, Toyama, Japan. The site is surrounded by 53 Japanese commercial power reactors. It was built to detect electron antineutrinos. Nuclear reactors produce electron antineutrinos $(\bar{\nu}_e)$ during the decay of radioactive fission products in the nuclear fuel. The experiment is sensitive up to ~25% of antineutrinos prediction emit from nuclear reactors. KamLAND gained 1.8 MeV of threshold energy by its experiment.

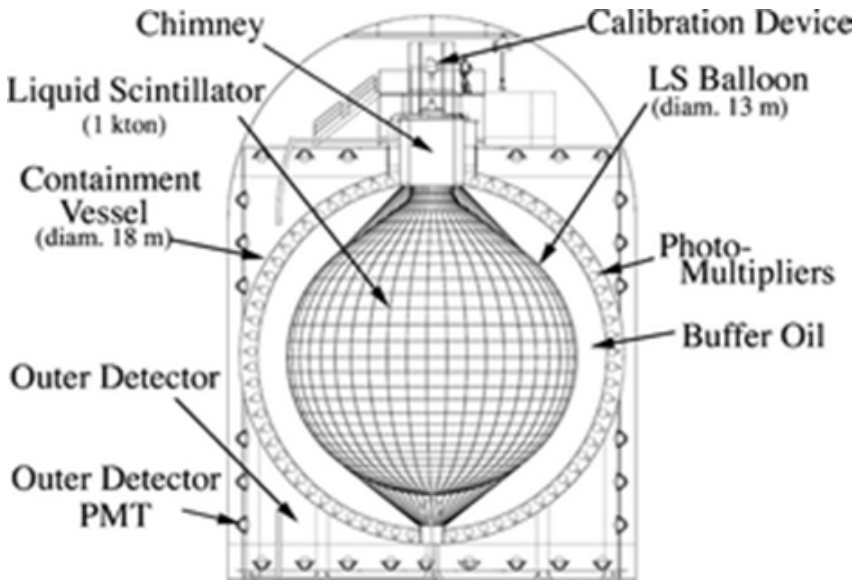

Figure 1.5 Schematic of the KamLAND detector

KamLAND consists of an 18 m diameter stainless steel spherical vessel, with (50 cm diameter) covered on its inner surface. The sphere is constructed with a 13 m diameter nylon balloon which is filled with liquid scintillator. The scintillator is formed by 1,000 metric ton of mineral oil, benzene and fluorescent chemicals acted as a shielding against external radiation.

The KamLAND experiment measures the total number of antineutrinos and their energy. The antineutrinos spectrum is consistent with neutrino oscillation and

contributes the values for the Δm^2 and θ parameters. Since KamLAND measures Δm^2 most precisely and the solar experiments exceed KamLAND's ability to measure θ, the most precise oscillation parameters are obtained by combining the results from solar experiments and KamLAND. Such a combined fit gives $\Delta m^2 = 7.9^{+0.6}_{-0.5} x10^{-5} eV^2$ and $\tan 2\theta = 0.40^{+0.10}_{-0.07}$, the best solar neutrino oscillation parameter determination to date. KamLAND also published a recent investigation of geo-neutrinos. These neutrinos are produced in the decay of thorium and uranium in the Earth's crust and mantle.

1.3.6 SNO

The Sudbury Neutrino Observatory (SNO) is a neutrino experiment located 2 km underground in Ontario, Canada. The detector is sensitive to all neutrino flavors and designed to detect solar neutrinos through their interactions with a large tank of heavy water. It consists of a spherical acrylic vessel and contains 1000 ton of high purity heavy water (D_2O). The water is surrounded by 7800 tons of ultra-pure water of shielding purposes. The experiment observed the light originated from relativistic electrons in the water which created by neutrino interactions. A neutrino converts the neutron in a deuteron to a proton. As relativistic electrons travel through a medium, they lose energy producing a cone of blue light through the Cherenkov effect, this light can be detected directly.

Figure 1.6 The concept of SNO's detector.

In the charged current interaction, a neutrino is absorbed in the reaction and producing electron. The emitted electron carries out most of the neutrino's energy, on the order of 5–15 MeV, and it was detectable. In the neutral current interaction, a neutrino dissociates the deuteron into a neutron and proton. The neutrino still emitted in the result with a slightly less energy. All types of neutrinos are possible to participate in this interaction. In the elastic scattering interaction, a neutrino collides with an atomic electron and imports some of its energy to the electron. All three neutrinos can arrange this interaction through the exchange of the neutral Z boson.

All interactions are dominated by electron neutrinos, which provided the first clear evidence of neutrinos oscillations (i.e. that they can transmute into one another). The total flux of all neutrino flavors measured by SNO is well agreed with the theoretical prediction. SNO's results were the first experimental data which calculate solar neutrinos oscillation directly.

1.3.7 The Problem on Solar Neutrino Experiments

Fusion reaction in the sun is generated by a proton–proton chain reaction. It converts four hydrogen nuclei (protons) into helium, neutrinos, positrons and energy. The excess energy is released as gamma rays, kinetic, and neutrinos. The solar neutrino has a problem in the area of flux measurement. It seem that a difference result between experimental and predicted value from SNU (Solar Neutrino Units). Almost experimental data are lower than theoretical models of solar interior. Eventhough neutrinos detector technology was highly sensitive. Main features of all solar neutrino experiments are listed in **Table 1.2**. All these experiments measures $\bar{v}_e$'s. Only SNO experiment can detect $\bar{v}_\mu$'s and $\bar{v}_\tau$'s through the elastic scattering reaction with approximately one sixth of the sensitivity to $\bar{v}_e$'s.

Table 1.2 Show the comparison features of the solar neutrino experiments.

Abbreviation	Sensitivity (a)	Type	Induced Reaction	Detector	Threshold Energy	Location and Year
BOREXINO	LS	ν_e	$\nu_x + e^- \rightarrow \nu_x + e^-$	LOS shielded by water	250-665 keV	Gran Sasso, Italy, 2007
GALLEX	LS	ν_e	$\nu_e + {}^{71}Ga \rightarrow {}^{71}Ge + e^-$	$GaCl_3$(30 t)	233.2 keV	Gran Sasso 1991-1997
HOMESTAKE	S	ν_e	${}^{37}Cl + \nu_e \rightarrow {}^{37}Ar^* + e^-$ ${}^{37}Ar^* \rightarrow {}^{37}Cl + e^+ + \nu_e$	C_2Cl_4(615 t)	814 keV	South Dakota, 1967-1998
Kamiokande	S, ATM	ν_e	$\nu + e^- \rightarrow \nu + e^-$	Water (H_2O)	7.5 MeV	Kamioka, Japan, 1986-1995
KamLAND	R	$\bar{\nu}_e$	$\bar{\nu}_e + p \rightarrow e^- + n$	LOS	1.8 MeV	Kamioka Japan 2002-
SNO	S, ATM	ν_e, ν_μ ν_τ	$\nu_e + {}^2D \rightarrow 2p + e^-$ $\nu_x + {}^2D \rightarrow \nu_x + n + p$ $\nu_e + e^- \rightarrow \nu_e + e^-$	Heavy water (1 kt D_2O)	3.5 MeV	Ontario, 1999-2006

(a) Solar neutrino (S), Low-energy solar neutrino (LS), Reactor neutrino (R), Atmospheric neutrino (ATM)

1.4 Purpose of This Research

Neutrinos have been measured[47] by using an electrochemical detector. The experiment was carried out for both thermal nuclear reactor and environmental neutrinos. On the basis of the experimental data, neutrinos were supposed[52] to consist of boson v_b and fermion v_f particles. Some biological materials were postulated to create the auxiliary field (B^0- field)[52]. When the B^0 field from biological material such as raw silk influences to low energy neutrinos, it may induce them to make transition into the reactive neutrino state. The neutrinos may also separate water molecule into hydrogen and hydroxide ions. The ions and neutrino fragments were considered to produce the output current. Although the signal generation scenario was proposed[47], quantitative analysis was not performed for the output current of the apparatus. In this study, a half-cell model with assistance of weak interaction is proposed to numerically calculate the output current of the apparatus. The same electrochemical parameters are employed for analyzing the previous experimental data.

The electrochemical apparatus tends to make a peak current at first a few days. The initial peak has a large variation in height in individual measurements. As one of possible reasons for the variation, it is interesting to consider the effect of solar activity. The solar activity has a periodicity of 28 days. Among the activity, the solar wind velocity also varies on the same periodicity. The solar wind has relationship to geomagnetism. The solar wind may affect geomagnetism and the transportation of low-energy geoneutrinos or their fragments. As a result by examining our data of the past half-year, we found a positive correlation between the solar wind velocity and the initial peak current. Therefore, we continue the experiment to study whether the correlation is true or not.

1.5 Overview of Subsequent Chapters

Chapter 2 describes the electrochemical detector, the physical and chemical properties of raw silk material, the selection criteria of working electrodes, the experimental process, and the proposed basic scenario of output current generation. Four experimental data are explained that will be analyzed in the next chapter.

Chapter 3 presents the electrochemical analysis of output current by using a half-cell model. The time evolution of output current is numerically solved with the half-cell model under the consideration of weak interaction effect. The same electrochemical parameters are applied to the four experiments. For the experiments with the use of water from silk-water mixture, the effect of the other cell was required on the voltage between the solution and electrode.

Chapter 4 describes the experiments on the poor-reproductive initial peak at a few days. The output current of electrochemical detector under environmental conditions gives an initial peak around 2 days and an equilibrium value in 2-3 weeks under environmental conditions. At early stage of our experimental study, a tendency of positive correlation was observed between the initial peak and solar wind velocity. Experimental study was continued to know whether the correlation is true or not.

Finally in Chapter 5, the conclusion of whole study is given, future prospect of neutrino study is also presented.

Chapter 2 Principle of Electrochemical Detector

2.1 Introduction

An electrochemical detector was proposed by our group to detect the low energy neutrinos. Biological material of raw silk is used for generating the auxiliary field which may influence neutrino to interact with water molecule. In this chapter, the principle of electrochemical detector, some physical and chemical properties of raw silk will be presented. The selection criteria's of working electrodes and electrode-pretreatment procedures, and important properties of the detector material will be described. The signal generation scenario will also be presented.

2.2 Experimental Apparatus

Figure 2.1 illustrates an electrochemical apparatus[47] for detecting low energy neutrinos.

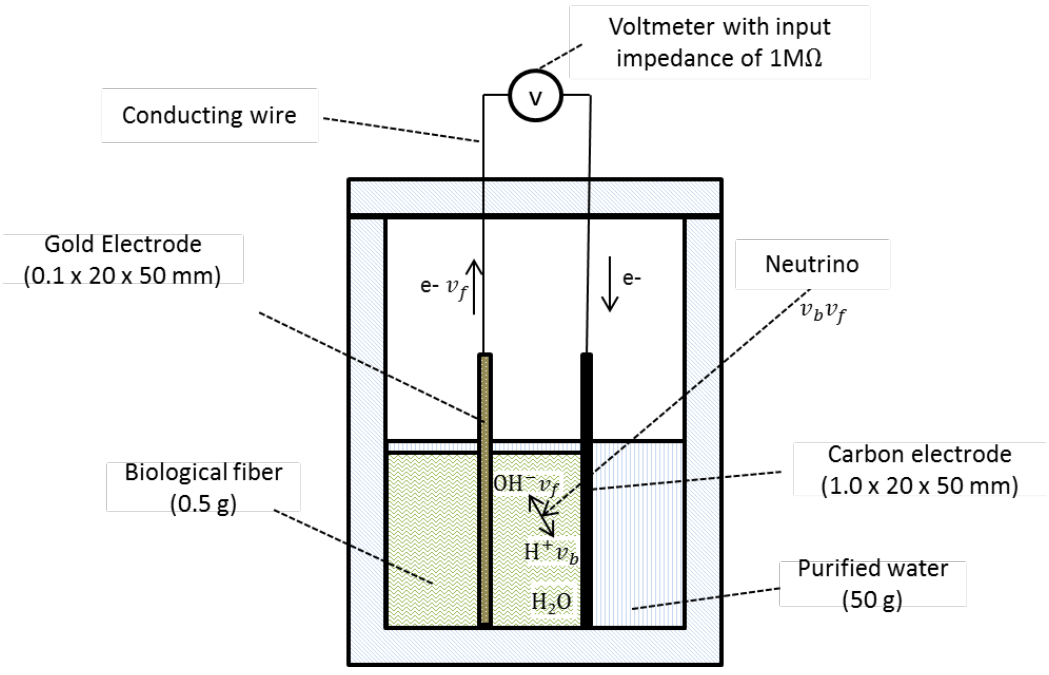

Figure 2.1 Schematic view of the experimental apparatus.

The experiment was set in a Teflon® Tetrafluoroethylene container of 90 mm in length and 58 mm in diameter. Purified water of 50 g was poured in its lower half region. Gold and glassy-carbon plates were used as the anode and cathode electrodes, respectively. They were both 20 mm x 50 mm in area. The thickness was 0.1 mm for the gold electrode and 1.0 mm for the carbon one. Electrodes were boiled in nitric acid for cleaning the surface. The electrodes were rinsed thoroughly in purified water by an ultrasonic washer. Purified water was bubbled by nitrogen gas before pouring the apparatus. The electrodes were placed in separation of 1 cm. Raw silk of 0.5 g in weight, chosen from biological material, was set on each side of gold electrode. The two electrodes were connected by copper wires to a voltmeter, where the input impedance was adjusted to be 1 MΩ with resistors. The value 1 MΩ was chosen from test experiments with input impedances of 0.3 to 4.5 MΩ. When the impedance was set, for example, at 0.3 MΩ the voltage decreased to almost half value, but the product of voltage and current, i.e. power, was kept the same as in the case of 1 MΩ. The output signal is expressed by the current in this study. The experimental apparatus was placed in an incubator to be operated at a temperature of 27^0C (300K). The reason for choosing each material to make the neutrino detector is briefly mentioned below.

2.3 Teflon Container

Teflon is the commercial name of the polymer polytetrafluoroethylene (PTEE), and it is composed of carbon and fluorine, with the molecular structure of $(-CF_2-CF_2-)_n$. The plastic Teflon are commonly used in various fields[37], and its important properties are:

1. Teflon is inert to all chemicals, acids, bases, organic solvents, high temperature and various kinds of radiations. Fluorine is the most electronegative atom, thus a high polar between fluorine and carbon. The fluorine atoms are held very close to the carbon atoms and the electrons around the fluorine atoms are held very tightly. In effect, the fluorine atoms act as a shield that prohibits other chemicals from reacting with the chain of carbon atoms. This results in a very inert polymer.
2. It has good thermal stability and good weather resistance. At 327^0C, it becomes a thick non-flowing liquid. above 327^0C Teflon simply decomposes. It remains

unchange at cryogenic temperature.

3. It is non-polar, non-toxic and will not corrode.
4. Teflon has outstanding electrical insulating properties, and of course its non-sticky properties are excellent.
5. It is insoluble in everything except fluorocarbon oils at very high temperatures.
6. Teflon is self-lubricating and its non-sticky properties correspond to its very low coefficient of friction.

Related to these features, Teflon has been used in many fields including in the laboratory. The experiment detector in this study is set up with Teflon.

2.4 Raw Silk

The raw silk is produced by boiling cocoon filament and the cocoon filament is composed of two proteins named fibroin and sericin, and matter such as fats, wax, sand pigments plus minerals. The composition of the cocoon filament is given below[38]:

Fibroin	: 72-81%
Sericin	: 19-28%
Fat and wax	: 0.8-1.0%
Coloring matter as ash	: 1.0-1.4%

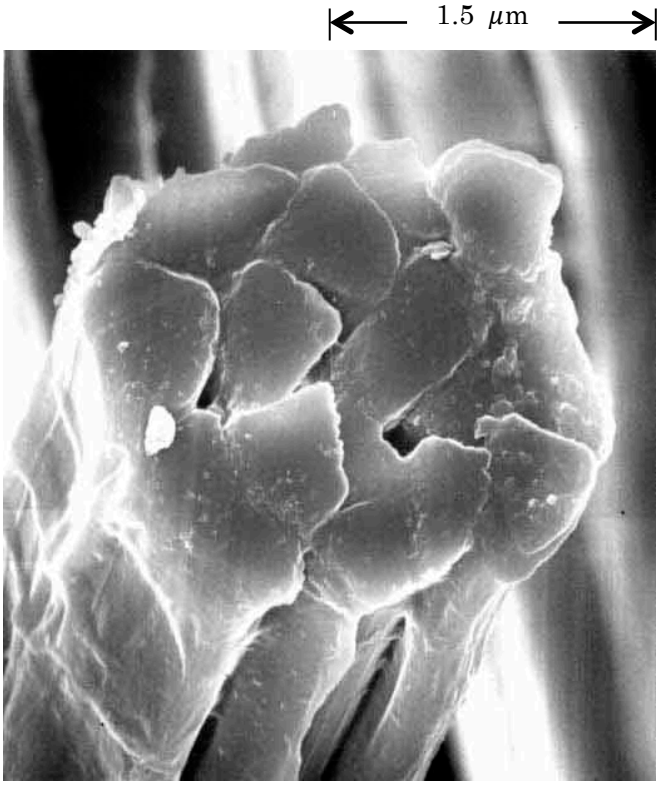

Figure 2.2 Cross section of raw silk thread (1,300 times by SEM)

The silk glands of the *Bomboyx mori* are structured like tube consisting of a posterior, middle and anterior section. the posterior is long and thin. The middle is short with a diameter measuring 3-4 mm. the anterior is extremely thin, leading to the spinneret in the heat of the larvae from which the silk is extracted[60].

Fibroin is secreted in the posterior and transferred by peristalsis to the middle section, which acts as a reservoir. Here it is stored as a viscous aqueous solution until required for spinning. The majority of the sericin is created within the walls of the middle section. In fact, these two proteins are reserved side by side in the middle section without mixing one into the other[60]. The fibroin core is covered with a layer of sericin and the secretions from the two proteins join at the junctions where the sericin is fused into one layer. The Filipis glands discharge a liquid protein. To form its cocoon, the silk worm draws out the thread of liquid protein and internally adds layer after layer to complete this protective covering[60]. **Fig. 2.2** shows the cross section of the raw silk thread.

The important physical and chemical properties are described below:

1) **Electrical Properties**: Raw silk is a poor conductor of electricity and readily accumulates a static electric charge from friction. This trait makes it difficult to handle in the manufacturing process. This static charge can be dissipated by high humadity.
2) **Specific Gravity**: the raw silk specific gravity on average of sericin and fibroin measures from 1.32 to 1.40[38]. Generally, the specific gravity of sericin is slightly higher than that of fibroin.
3) **Effect of Light**: Continuous exposure to light weakens silk faster than cotton or wool. Raw silk is more resistant to light than other silks. Raw silk drapery and upholstery fabrics are protected from direct exposure to the light.
4) **Action of Water**: Silk is a highly absorbent fiber, which readily becomes impregnated with water. Water, however, does not permanently affect silk fiber. Silk strength decreases about 20 percent when wet and regains its original strength after dying. The fiber expands but does not dissolve wen steeped in warm water.
5) **Degradation by Acids and Alkalis**: Treatment of the raw silk fibers with acid or alkaline substances causes hydrolysis of the peptide linkages. The degree of hydrolysis is based on the pH value, which is at minimum between 4 and 8. Degradation of fiber is exhibited by change in the viscosity of the solution. Hydrolysis by acid is more extensive than alkali, and it has been postulated that acid hydrolysis occurs at linkages widely distributed along the protein chain, whereas in the early stages of the alkaline treatment, hydrolysis happens at the end of the chain.
6) **Oxidation**: Reports regarding the oxidation of protein are rather meager since the reactions are very complex. Oxidation agents may attack proteins in three possible points :
   - at the side chains,
   - at the N-terminal residues, and
   - at the peptide bonds of adjacent amino groups.

2.5 Working electrode

From the electrochemical views, when the positive and negative electrodes are placed into an electrolyte solution, the positive and negative ions of this electrolyte are move to the two electrodes, anode and cathode. Anode serves the oxidation reaction by injecting a negative charge into electrolyte solution. While cathode works for the reduction reaction by accepting an electron charge from the solution. Then current from either reduction or oxidation is induced in the outer circuit of electrolytic cell. It can be written as follows

Cathode : $X + e^- \rightarrow Y$ (reduction reaction) (2.1)

Anode : $Y \rightarrow X + e^-$ (oxidation reaction) (2.2)

where X and Y are oxidizing and reducing, respectively. The transfer process of electron and its rate in the electrolytic solution is related to the physical and chemical properties of the electrode material. Studies of the oxidation of hydrocarbon[43] and reduction of water and hydrogen ion[44] by electro-catalysis have provided sample evidence for its existence. Thus, the selection of the electrode materials depends on the following factors.

1) The material should be irresponsible to the electrochemical interaction, but only offering the place to the reaction and holding a wide electrical potential.
2) It does not dissolve into the solution and also not produce oxide film.
3) The surface should be easy to be clean.
4) The material surface should be homogeneous with a large cross sectional area for interaction.
5) Other analysis includes the hydrogen overvoltage, oxygen overvoltage and toxicity.

A standard electrode potential is used to determine the equilibrium potential of electrode, where the temperature and pressure are 25 ^{0}C and one atmospheric. It is

applied for either the oxidation or reduction reaction in electrode. Usually, the standard hydrogen electrode (SHE) is applicable as a reference for the purpose.

$$\begin{array}{l}\leftarrow \text{anode reactions} \\ 2H^+ + e^- \Leftrightarrow H_2 \\ \rightarrow \text{cathode reactions}\end{array} \qquad (2.3)$$

According to the potential factor, anode is defined when the potential is positive comparing with the SHE. It is caused by oxidation of H_2 into ion H^+, if the eq. (2.3) goes to the left hand side. In contrast, cathode is assumed when the electrode potential is less than SHE and defined as zero. Meaning that, the potential of this electrode is negative. It occurs if hydrogen ion (H^+) in eq. (2.3) is converted into H_2 in the right side.

Theoretically, the reduced current can be observed when negative potential appears on the electrode. Otherwise, the oxidized one is observed for positive potential on the electrode. In some cases, the reduced current can not be observed eventhough negative potential appears on the electrode. It considers to the presence of an overvoltage for one electrode that consists of the hydrogen and oxygen ones. The reduction reaction of hydrogen ion in eq. (2.3) is also take place in the electrical potential of

$$E = E_{H/H_2^0} - 0.059\,pH \qquad (2.4)$$

The equation (2.4) implies that the range of electrical potential varies with only the pH value. Meanwhile, the variation of electrical potential is in appropriate with the variation of electrode materials. Hence, the difference between the theoretical and observed electrical potential is defined as the hydrogen overvoltage. On the basis of eq. (2.4), one shows that the hydrogen overvoltage is increasing in order of electrodes like Pt, Pd, Ru, Rh, Au, Fe, Co, Ag, Ni, Cu, Cd, Sn, Pd, Zn, and Hg. Both Pt and Pd have extremely small hydrogen overvoltage, which is the basis for their use in the constraction of reversible hydrogen electrodes. However, Gold has a larger overvoltage, in spite of much smaller than mercury.

Similarly to the oxygen overvoltage, it assumed as the difference between the theoretical and observed electrical potential for oxygen to produce in an electrical solution. And also it varies with different electrodes. The oxygen overvoltage changes in the order of electrodes as Ni, Fe, Pb, Ag, Cd, Pt, and Au. Analogy with the hydrogen overvoltage, one can infers that Au and Pt are widely used as the anode electrodes for the oxidation reaction.

2.5.1 Anode

Accordingly, solid electrodes with extended anodic potential windows have atracted considerable analyically interest. An important factor in choosing electrodes is the dependence of the response on the surface state of the electrode. Gold is the most widely used metallic electrode. It is readily obtained in high purity, easy to be machined, and can be fabricated readily into a variety of geometric configurations.

Gold is very difficult to absorb hydrogen. In particular, the absorption and desorption reactions of hydrogen do not appear in the gold electrode. It means the hydrogen evolution is difficult to occur in the gold electrode. Moreover, gold electrode has an high oxygen overvoltage. This feature is suited to be used as the anode in oxide reaction. For this reason, the gold plate is selected to be used as anode in the experimental apparatus.

2.5.2 Cathode

Carbon electrodes are used widely in electroanalysis, primarily because of their characteristics: broad potential window, low background current, chemical inertness, and suitability for various sensing and detection applications. The most populer carbon electrode materials are those involving glassy carbon, carbon paste, carbon fiber, screen-printed carbon stripd, carbon films, or other composites.

The use of glassy carbon as an electrode material was first suggested by Yamada and Sato[40] in 1962. The glassy carbon has been very popular proprietary material[39] because of its excellent mechanical electrical properties, wide potential window, high conductivity, impermeable to gases, high resistant to chemical attack, and

reproducible performance. Glassy carbon is selected to use as the cathode in the experiment apparatus.

2.5.3 Electrode Pretreatment

Solid electrodes have been studied extensively. They provide a larger potential range than mercury, have better mechanical properties and can play as a catalytic role for electro-synthesis and electro-analysis reactions. The pretreatment procedure will affects the solid electrode behavior related to the change in the heterogeneous electron transfer rate, increase in capacitance or surface Faradic reactions[42, 41]. In most cases, the electrode behaviour is degraded with time due to absorption of impurities from the solution or chemical changes to the electrode surface, and the solid electrode becomes unsuitable for quantitative measurements.

A variety of methods have been devised for pre-treating solid electrodes, including polishing, chemical pretreatment, flaming, vacuum heat treatments and ion etching[49]. These procedures produce widely varying effects on charge transfer rate, mainly because they vary greatly in the resulting degree of surface cleanliness. There is no standard procedure for preparing solid electrode surfaces, and pretreatments vary greatly from lab to lab. The following steps are applied for the pretreatment of gold and glassy electrodes used in experiment.

1) Surface of glassy carbon electrodes is made smoothly and brightly with fine getar paper.
2) Electrodes are placed in a beaker with water and then washed in an ultrasonic bath. The water in the beaker is changed several times. Ultrasonication time is 15 min.
3) The electrodes are thoroughly rinsed prior to each step. Electrodes are boiled with HNO_3 for typically 15 min.
4) Electrodes are washed with purified water following the second step for many times until the pH of the water that has been used to washed the electrodes becomes neutral.
5) The two electrodes are immersed in the same purified water and stored until the experiment.

2.6 Experimental Water

The earliest requirement for the pure water is in electrochemical research; attainment of lowest conductivity and neutrality (pH) are of primary concern. It has been universal practice to assess the quality of pure water by measurement of its specific conductivity.

Natural water is electrically conductive due to some minerals and impurities. But The process to make pure water by removing electrolytes will effect in decreasing its conductivity. Indeed, ultra-pure water is highly non-conductive and such water is prepared by ion-exchanged technique. When this water comes in contact with air, carbon dioxide is dissolved in water, causing its conductivity to rise. This does affect the conductivity of pure water. In order to carry out the present study, purified water is used in the experimental detector. This purified water was bought from Takasugi Seiyaku co. Ltd., Japan, and it's produced through the following procedure.

1. Distillation water passes through an ion-exchange column.
2. The water (1) is distillated again.
3. The distillation water (2) passes through the second ion-exchange column again to form the purified water.

2.7 Experiment

This study analyzes four experimental data. The first experiment is measured in a laboratory of Kyushu university (Hakozaki campus) under natural environmental circumstances. The output currents were counted from the input voltage by being divided by the impedance $1\mathrm{M}\Omega$. The measurement was carried out with three apparatuses, and the experimental data[47] are plotted by three kinds of marks in **Fig. 2.3(1)**. The variation in three measurements was 3% in one sigma.

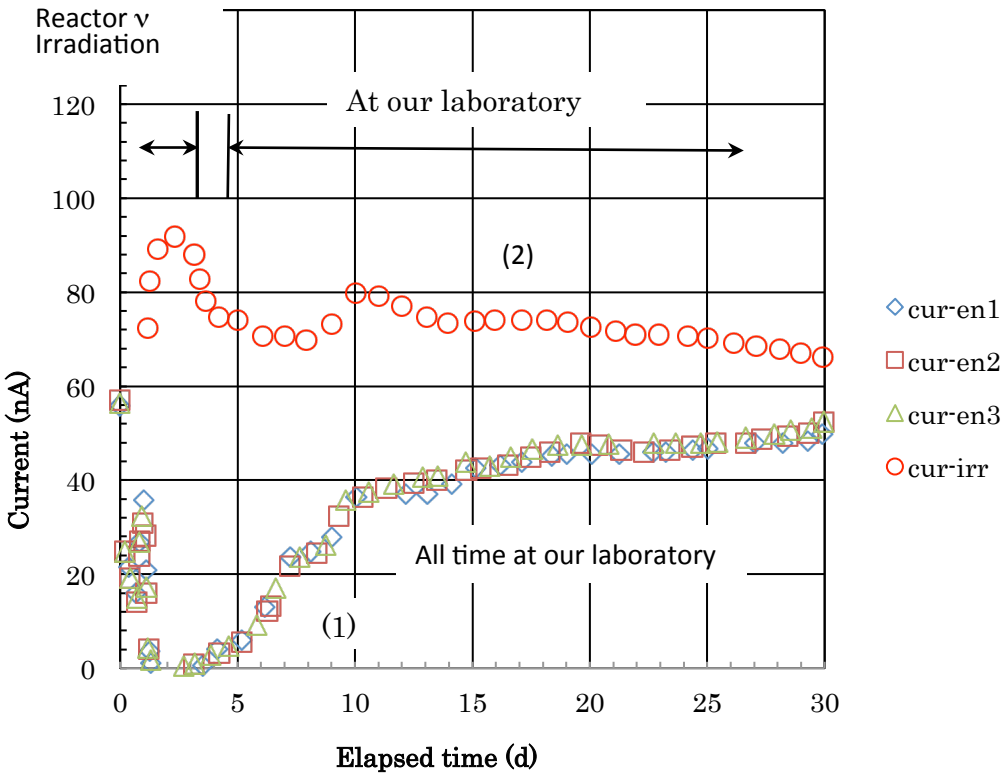

Figure 2.3 Output current of the experimental apparatus. The lower marks of three types are the results for the experiments performed under environmental conditions in a laboratory at Kyushu University, while the upper marks show the results obtained under reactor-neutrino irradiation and subsequent environmental conditions[47].

The initial peaks appear at 1.5 days. After the initial peak, the current signals fell to almost zero values. Then they gradually increased, and subsequently reached about 50 nA after 20 days. When the experiment was made without raw silk, the current fell[47] to zero within a day. In the case of use of other artificial fibers, the current also went to zero completely in few to several days[47].

The second experiment was carried out at the site of nuclear thermal reactor (electric power of 165 MW). The irradiation was made for three days at a distance of 35 m from the center of the reactor core. The antielectron neutrino flux was estimated to be 6.8×10^{11} $cm^{-2}s^{-1}$. The radiation dose in the experimental room of the irradiation was twice larger than natural radiation dose, that is, the experimental room was well shielded from neutrons and gamma rays. After irradiation, the apparatus was

transported to the laboratory of Kyushu University. The experiment was continued there. The results[47] are shown in the **Fig. 2.3(2)**. It is noted that the first and the second experiments were initiated simultaneously at the same time. The output current attained 90 nA in a day. It then decreased during the transportation and later time, but began to increase again after a week. The increased output signals was lost completely within several days. It is natural to consider that the larger currents in the **Fig. 2.3(2)** are ascribed to reactor antineutrinos. This suggests that the current in the **Fig. 2.3(1)** may also be caused by natural antineutrinos.

The third experiment was carried out by the use of water from mixture of silk and water. A bottle with 100 g of raw silk inside was poured by 800 g of water, the bottle and raw silk were stored for one month at the laboratory. After one month, the raw silk was taken out from the water. Then water and new raw silk were used to make the experiment. The measurement data of the forth experiment are plotted in **Fig. 2.4(3)**.

The current peak reached 60 nA at the second day. Then it was increased, and attained 140 nA after two weeks. The use of mixture water is considered as the reason for the difference between **Fig. 2.3(1)** and **Fig. 2.4(3)**.

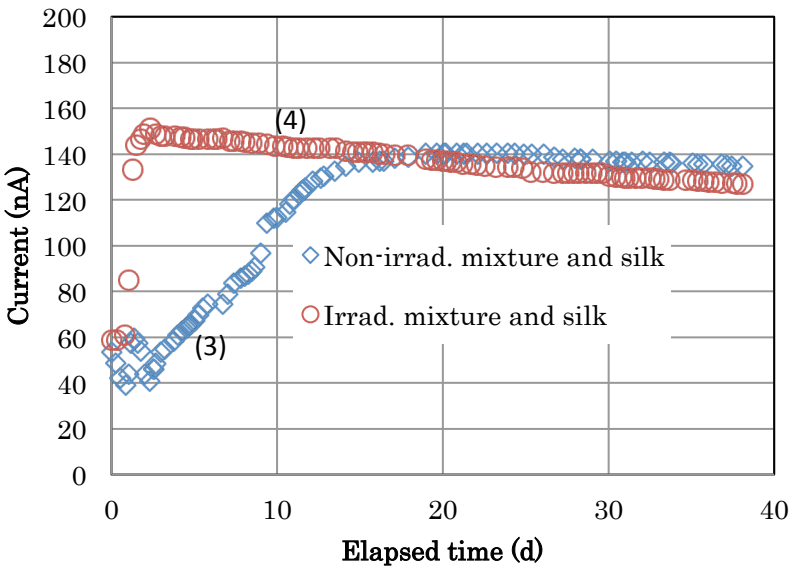

Figure 2.4 Output current of the experimental apparatus. The lower marks are the results for the non irradiated mixture water and non irradiated raw silk experiment, while the upper marks show the results obtained for irradiated mixture water and irradiated raw silk experiment[47].

The fourth experiment was carried out with irradiated water and irradiated raw silk. A bottle with 100 g of raw silk inside was poured by 800 g of water was placed at a position of 15 m from the core thermal nuclear reactor. Beside the bottle, a polyethylene bag containing fresh raw silk was also put there. The bottle and bag were irradiated by anti-electron neutrino for three days. Then they were taken and kept at the laboratory. The water from the bottle and the raw silk from the bag were used to make the experiment. The third and fourth experiments were started at the same time. Current output of the experiment is presented in **Fig. 2.4(4)**.

The curve of the experiment produces a higher current than other experiments. It achieved 150 nA at the fourth day. The current only decrease by 20 nA after three weeks. The reason is ascribed to the irradiation of reactor neutrinos.

2.8 Electrochemical Reactions

The electrode materials in the experimental apparatus are stable against most chemical reactions. In previous experiments[52,53], (a) ICP mass measurements indicates that the density of solved ions from raw silk saturated within a few days, and (b) the direct measurement of oxygen gas showed that the output current increased with oxygen gas concentration. In the **Fig. 2.3(2)**, the current glows quite immediately after being set near the nuclear reactor. This is not understood by the reduction and oxidation by oxygen gas at all. In the **Fig. 2.3(1)**, the signal gradually increases within a few weeks. This behavior disagrees with the above experimental indication (a). The carbon material is often utilized as a reduction electrode for phosphoric-acid fuel cells[51], and works for the electrochemical reaction of $4H^+ + O_2 + 4e \rightarrow 2H_2O$. The result (b) suggests the promotion of this kind of reaction in the apparatus.

The principle of neutrino detection is shown in **Fig. 2.5**. Suppose that hydrogen ion (H^+) and hydroxide ion (OH^-) are produced by the dissociation of water molecule. The separation energy[45] is written by

$$\Delta G = -RT\ln([H^+][OH^-]), \tag{2.5}$$

where R is the gas constant, 8.314 $JK^{-1}mol^{-1}$, and T is the temperature, 300K, and the scaled hydrogen ion and oxygen ion concentrations are similar at 1 x 10^{-7} mole perliter purified water. When a water molecule is dissociatively ionized into hydrogen ion (H^+) and hydroxide ions (OH^-), the threshold energy for the reaction is 0.84 eV. It was presumed that the raw silk produces scalar auxiliary field $B^{0(50)}_{\nu_b \nu_f}$. A neutrino is postulated[50] to be composed of boson and fermion particles as .

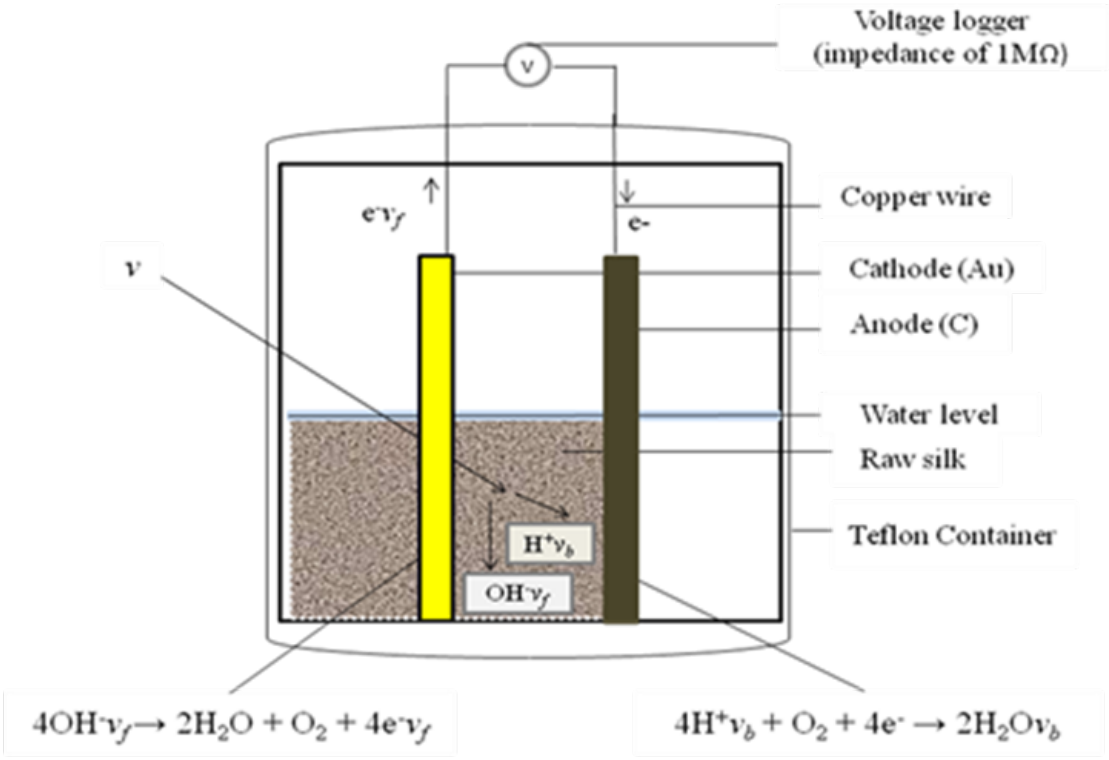

Figure 2.5 Experimental apparatus with explanation of proposed charge transfer process.

When the field energy of B^0 from the raw silk is large, it may increase the neutrino mass and make the neutrino unstable[50]. The signal generation scenario is as follows [52]. The neutrino may make a water molecule to separate into hydrogen and hydroxide ion through the dissociative ionization as

$$v_b v_f + H_2O \rightarrow H^+ v_b + OH^- v_f \quad (2.6)$$

The hydroxide ions generates oxygen gas with transferring $e^- v_f$ pairs to the electrode as

$$4OH^- v_f \rightarrow 2H_2O + O_2 + 4e^- v_f \quad \text{(anode reaction)} \quad (2.7)$$

The hydrogen ions with boson ($H^+ v_b$) in eq. (2.6) may move to the carbon plate. The oxygen gas generated in eq. (2.7) may also arrive at this electrode, where $H^+ v_b$ and O_2 receive the charge e that conducts through the connecting wire. The reduction reaction on the carbon electrode is given as

$$4H^+ v_b + O_2 + 4e^- \rightarrow 2(H^+ v_b)_2O. \quad \text{(cathode reaction)} \quad (2.8)$$

This reaction is considered to keep the bound state between hydrogen and boson. Thus, the hydrogen and hydroxide ions in eq. (2.6) were understood to produce water molecules, causing the charge transfer between electrodes. Similarly in the case of conventional OH^- and H^+ ions. eqs. (2.7) and (2.8) are considered to be endothermic and exothermic reactions, respectively. The reaction of eq. (2.7) is promoted by some catalyst effect related to the weak interaction by B^0. When this works, diffusions of ions and gas related to eqs. (2.7) and (2.8) are expected to take place to produce the current through the conduction wire.

These results are concerned with the low energy antielectron neutrinos, which may have a size of internal structure comparable to atomic diameter. The antielectron neutrinos, for example, below 50 keV, have a fraction[46] of 8.0 x 10^{-3} to the total reactor neutrino flux. The natural radiations contain antielectron neutrinos, i.e. geoneutrinos. The geoneutrinos are generated in the interior of the Earth mainly from the progenies of $^{238,235}U$, ^{232}Th and ^{40}K decays. The flux of geoneutrinos below 50 keV, for instance, was calculated by KAMLAND group and found to be 5.7 x 10^5 $cm^{-2}s^{-1}$ under the assumption of typical global abundances[47]. The ratio of the

low-energy antielectron neutrino flux in the upper to that in the lower ones during the first three days was evaluated to be 9.5×10^3. It is interesting to study whether the four responses are quantitatively understood with basically the same procedure or not.

Chapter 3. Electrochemical Analysis

3.1 Half-cell model

On the basis of the process in eqs. (2.7 - 2.8), this study attempts to describe the time response evaluation of the output currents in **Fig. 2.5**. The usual formulation of electrochemical reaction in a standard text book[54] is adopted as a half-cell model, but the effect of the weak interaction is considered. For a reversible reaction on the carbon electrode, the current density j is written by using the reduction reaction rate v_c and the oxidation one v_a as

$$j = nF(v_c - v_a) = j_{H^+} + j_{H_2O}, \tag{3.1}$$

where n is the number of moving electrons in the reaction and F stands for the Faraday constant $F = eN_A$ with e the electron charge and N_A the Avogadro number. The reduction reaction rate is expressed by

$$v_c = P_c[H^+ v_b]^4[O_2]\exp\left(-\Delta G^{\neq}/RT\right), \tag{3.2}$$

where P_c stands for the reaction rate coefficient, R the gas constant, T the temperature and $\Delta G^{\neq}$ the free energy of activation. The bracket [ ] indicates concentration thereafter. The value of $\Delta G^{\neq}$ takes the form of

$$\Delta G^{\neq} = \Delta G^{0\neq} + \alpha nFE, \tag{3.3}$$

where $\Delta G^{0\neq}$ is the activation energy at zero bias voltage, E the bias voltage and α the transfer coefficient. Therefore, the current density j_{H^+} is given by the Butler-Volmer equation[54] as

$$j_{\mathrm{H}^+} = nFP_c[\mathrm{H}^+ v_b]^4[\mathrm{O}_2]\exp\left(-\frac{\Delta G^{0\neq} + \alpha nFE}{RT}\right), \tag{3.4}$$

where n is set at 4 according to eq. (2.8). Since the current is written as $I_{\mathrm{H}^+} = j_{\mathrm{H}^+} A$ with area A, the use of $\Delta G^{0\neq} = N_A \Delta$ in eq. (2.8) leads to

$$I_{\mathrm{H}^+} = 4FAP_c[\mathrm{H}^+ v_b]^4[\mathrm{O}_2]\exp\left(-\frac{\Delta + 4\alpha eE}{k_B T}\right), \tag{3.5}$$

where k_B is the Boltzmann constant, and e the electron charge. Similarly, the density of water molecule may produce another current by the reverse reaction as

$$I_{\mathrm{H_2O}} = -4FAP_a[\mathrm{H_2O}]^2\left(-\frac{\Delta - 4(1-\alpha)eE}{k_B T}\right). \tag{3.6}$$

The oxidation electrode in eq. (2.7) gives rise to the endothermic reaction (Q = – 0.40 eV). Therefore, the reaction in eq. (2.7) is incapable of inducing the oxidation reaction without assistance such as catalyst. When the raw silk is present around the gold electrode, the energy difference of B^0 field between the regions inside and outside the gold plate may supply an energy compensating to the exothermic reaction. In this case, eq. (3.1) on the carbon electrode is supposed to determining the current as the half-cell model.

As an additional reaction, positive ions of Ca^{2+} and Mg^{2+} were present[47] in the solution. Such ions were solved out from the raw silk into water. An impurity current I_{imp} is treated to be produced by a simple reduction reaction, and be formulated as

$$I_{\mathrm{imp}} = 4FAP_i[\mathrm{M}^{2+}]^2[\mathrm{O}_2]\exp\left(-\frac{\Delta + 4\alpha eE}{k_B T}\right) \quad . \tag{3.7}$$

The value of Δ is set at the same value in eq. (3.4), but is actually corrected by the coefficient P_i with adjustable feature. The reverse current for I_{imp} is neglected in this study. Thus, the induced current becomes $I = I_{\mathrm{H}^+} + I_{\mathrm{H_2O}} + I_{\mathrm{imp}}$ with regard to the

carbon electrode with the half - cell model. The current I_{H_2O} is mostly negligible in the electrochemical experiment in this study.

3.2 Output current analysis by the half-cell model

The experimental results in **Figs. 2.3 - 2.4** are analyzed by using the half-cell model. The concentration [$OH^- v_f$] is implicitly taken to be the same as [$H^+ v_b$] because of assumption of the same rate in eqs. (2.7) – (2.8). For simplicity, as for the impurity current in eq. (3.7), the oxidation reaction of negative ions is assumed to take place for compensation around the gold electrode, although they are not presented explicitly in the equations. Under these circumstances, the half - cell model is applied to the analysis.

3.2.1 Free energy of activation Δ

The electrochemical current depends strongly on temperature. This relation is written in terms of logarithmic function as

$$\ln I = \ln I' - \frac{\Delta G^{0\neq}}{RT}. \tag{3.8}$$

The activation energy is obtained by the experimental data[50]. The experiments were performed at various temperatures and the data are listed in **Table 3.1**. An Arrhenius plot of current versus temperature shows a linear correlation in **Fig. 3.1**, and gives Δ = 0.65 eV.

Table 3.1 Experimental output current as a function of temperature under environmental conditions.

Temperature T(K)	290	300	310
Stable current I(nA)	20.0	57.5	104.2

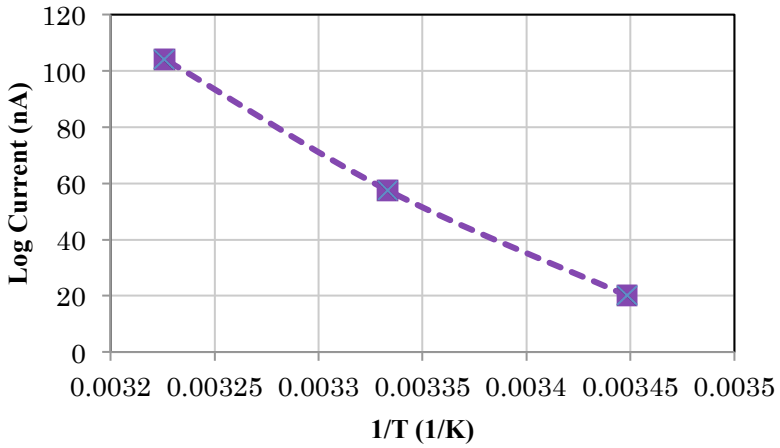

Figure 3.1 Correlation of output current and temperature.

3.2.2 Hydrogen-ion concentration

The reaction rate of antineutrino-water interaction is given by $R_{\mathrm{H_2O}} = \rho\sigma\varphi_v$, where ρ is the number density of water molecules, σ the cross section for the dissociative ionization and φ_v the antielectron neutrino flux of concern. The hydrogen ion concentration $[\mathrm{H}^+ v_b]$ is set at zero at the beginning and then increases by the dissociative ionization of water as B^0 glows in water by the solve out sericin from raw silk. The increasing rate is assumed to take a form of

$$[\mathrm{H}^+ v_b]_{rate,inc} = R_{\mathrm{H_2O}}(1/2)\{1+\tanh((t-t_d)/t_r)\}, \tag{3.9}$$

where $R_{\mathrm{H_2O}}$ indicates the reaction rate of dissociation of water, i.e. the product of water-molecule number density, neutrino flux of concern and cross section in eq. (2.6). The delay factor on $R_{\mathrm{H_2O}}$ includes time parameters t_d and t_r which express the delay and rising times in a function form of 1+tanh respectively. The delay factor is introduced to express the solved-out time of materials from raw silk in soak, and the transient effect of diffusions of ions and oxygen gas in eqs. (2.7) and (2.8). The hydrogen ions should disappear by the rate of I/F as the current I in eq. (3.1) flows.

The ion concentration is assumed to be formed uniformly in the cell of apparatus. The decreasing rate of hydrogen ion concentration is written as

$$[\mathrm{H}^{+}v_b]_{rate,dec} = -I/VF, \tag{3.10}$$

where V is the volume of working cell, I is the current. The sum of eqs. (3.9) and (3.10) determines the variation of hydrogen ion concentration in the reaction. Therefore, the current density $j_{\mathrm{H}^{+}}$ in the Butler-Volmer equation in eq. (3.4) is influenced by variation of $[\mathrm{H}^{+}v_b]$ through the sum of eqs. (3.9) and (3.10).

3.2.3 Oxygen gas concentration

The oxygen gas concentration relative to the saturated value in water was measured[52] by our group. The relative concentration was 8% immediately after starting of experiment. It considerably decreased to almost zero value in 3 days, and started to increase and reached 12% in 17 days. This indicates that the oxygen gas was generated by certain processes. The oxygen gas may be generated from either a direct process in the antineutrino-water reaction or recombination of $\mathrm{H}^{+}v_b$ and $\mathrm{OH}^{-}v_f$ under the influence of B^0 field supposedly around the gold electrode. However, we regard the recombination effect to be considered in the direct reaction, as the simplest approximation. Introduction of a fraction k_{O_2} to $R_{\mathrm{H_2O}}$ leads to

$$[\mathrm{O}_2]_{rate,inc} = k_{\mathrm{O}_2} R_{\mathrm{H_2O}} (1/2)\{1 + \tanh((t - t_d)/t_r)\}. \tag{3.11}$$

The oxygen gas concentration increases according to this equation, while it decreases with the reduction reaction of impurity ions in eq. (3.7).

3.2.4 Voltage across the carbon electrode

The electric voltage between gold and carbon electrodes is expressed as IR, where I is the output current and R the input impedance of the voltmeter. The voltage E between the carbon electrode and the solution may be given by $E = IR + E_{AU}$, where E_{AU} serves as the correction of E and is mainly the potential difference between the gold electrode and the solution. We set at $E_{AU} = 0$ for experiments in **Fig. 2.3**. The experiments were performed at the temperature T = 300K, so that k_BT = 0.0259 eV. The carbon plate area A was 7 cm^2.

3.3 Fitting of the experimental results

Calculations were performed for the currents in **Figs. 2.3 - 2.4**. For the environmental experiment in the **Fig. 3.2(1)**, the current - fitting computations were made with the constraint where the experimental behavior of oxygen gas concentration was taken into account. The fitting with $I = I_{H^+} + I_{H_2O}$ except I_{imp} represented the gradual glow of currents after 3 days, but did not reproduce the initial current peak at all. This suggests that impurity ions were solved out from the raw silk and they produced the initial peak by consuming oxygen gas. For this reason, the fitting was made by employing $I = I_{H^+} + I_{H_2O} + I_{imp}$, and the results are drawn with a solid curve in the **Fig. 3.2(1)**. The calculated values are somewhat larger at 5-6 days than the experimental data. This may be ascribed the simple constant value of k_{O_2} in eq. (3.11). The parameters are listed in **Table 3.2**.

The most important parameter in the electrochemical model is the reaction rate coefficient P_c. The phosphoric-acid fuel cells basically make use of the reaction similar to eq. (2.8). Since there is the difference in catalyst and operation temperature between the fuel cells and the present apparatus, the validity of P_c is not able to be discussed directly. The values of t_d and t_r , namely few days, were treated as adjustable parameter for expressing initiation of beginning point of weak-interaction assistance. The ICP mass measurement of ions in solution indicated that it took a few

days for ions such as Ca^{2+}, Mg^{2+} to solve out into water. In addition, transient diffusion effect should appear hydrogen and hydroxide ions and oxygen corresponding to eqs. (2.7) and (2.8). The values of T_d and T_r are considered to include these effects. The parameters P_c, P_a, P_i, R_{H_2O} and k_{O_2} were fixed in all simulations.

Table 3.2 Parameters in the half-cell model analysis.

$P_c = 1.4 \times 10^{34}$ cm^{13}mol^{-5}s^{-1}	$R_{H_2O} = 2.24 \times 10^{-13}$ mol cm^{-3}s^{-1}	$k_{O_2} = 0.12$
$P_a = 1 \times 10^{-3}$ cm^{4}mol^{-2}s^{-1}	$[M^{2+}] = 2.04 \times 10^{-9}$ mol cm^{-3}	$T_d = 2.00$ d
$P_i = 4.75 \times 10^{25}$cm^{7}mol^{-3}s^{-1}	$[O_2]_{ini} = 1.09 \times 10^{-9}$ mol cm^{-3}	$T_r = 1.20$ d

The parameters listed in **Table 3.2** were applied for the analysis of the first and the second experiments. For the third and fourth experiments, the concentration of ions and oxygen gas were taken to be adjustable in the calculation together with the time parameters T_d and T_r.

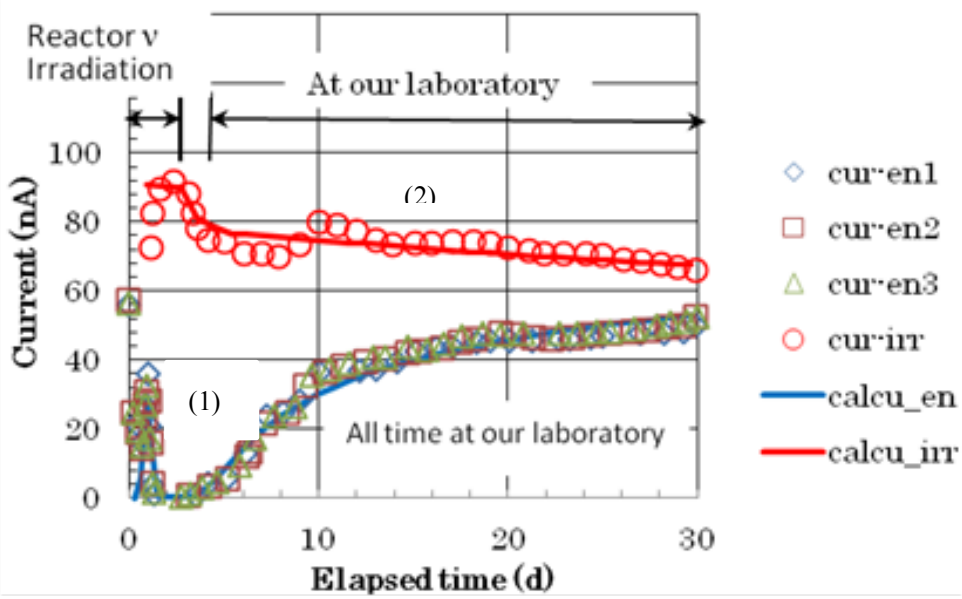

Figure 3.2 Calculated output current versus time. The lower curves of three types are the calculation results for the experiments performed under environmental conditions in a laboratory at Kyushu University, while the upper curves show the results obtained under reactor-neutrino irradiation and subsequent environmental conditions[47]. The solid curves indicate calculation results.

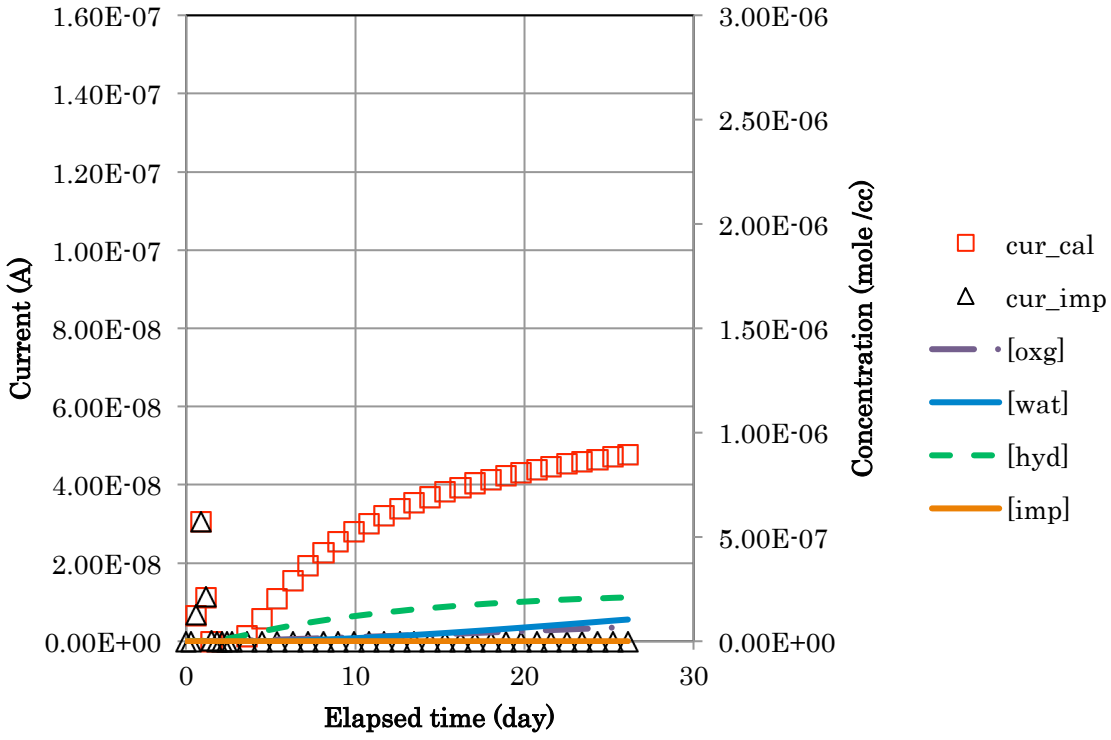

Figure 3.3 Detailed results of calculation current and concentrations for the environmental experiment at Kyushu University.

The impurity current and concentrations of ions are plotted in **Fig. 3.3**. One can see that the initial peak around 1.5 days is ascribed to the reduction of impurity ions shown by the impurity current as eq. (3.7). The initial peak current decreases soon as the oxygen gas concentration goes to zero. According to eq. (3.5) with $E = IR$, the observed current depends dominantly on the product $P_c[\mathrm{H}^+ \nu_b]^4[\mathrm{O}_2]$. The concentration variation rate of hydrogen ion increases by the dissociative ionization (eq. (3.9)) and decreases by the recombination into water (eq. (3.10)), while that of oxygen gas is generated with eq. (3.5). **Figure 3.3** indicates that the hydrogen ion concentration gradually glow due to eqs. (3.9) and (3.11), and that of oxygen gas also slowly increases.

Subsequently, the current in eq. (3.5) increases up to about 50 nA. The current $I_{\mathrm{H_2O}}$ by the oxidation reaction also flows in the carbon electrode as in eq. (3.6). This reaction is less important and negligible in most cases except the time period around 3

days. The output current increases as the accumulation of hydrogen ion and oxygen in the apparatus as inferred from eq. (3.5). Oxygen gas and hydrogen ion concentrations reach almost equilibrium value after 2-3 weeks. The comparison between the experiments and calculations suggests that the half-cell model works well for the environmental experiment.

The same parameters in **Table 3.2** may be applicable to the reactor-neutrino irradiation experiment, by correcting antineutrino flux by a factor of 9.5×10^3 during the first 3 days. However, the calculation produced the output current twice as large as the experimental data of 90 nA at a few days. The experimental current there seems to be saturated for a certain reason.

A limited value was set at 9.28×10^{-7} mol cm^{-3} for the hydrogen concentration $[H^+ v_b]$, and it was useful to reproduce the current saturation at a few days. Nevertheless, subsequently the calculated current slowly decreased down to 78 nA at 30 days. However, the output current was steeply reduced during the transportation to Kyushu University and later kept to a low value. This suggests that the vibration of the apparatus during the movement may decreases the concentration of ions and oxygen in the reaction cell. For this reason, the concentration of ions and oxygen were adjustably reduced to fit the experimental value during the transportation period. The calculation results are drawn in **Fig. 3.2(2)**. They fit the experimental data as a whole, but the variation around 10 days fails to be reproduced. The value E_{AU} may deviates from zero, but it was not considered in this study.

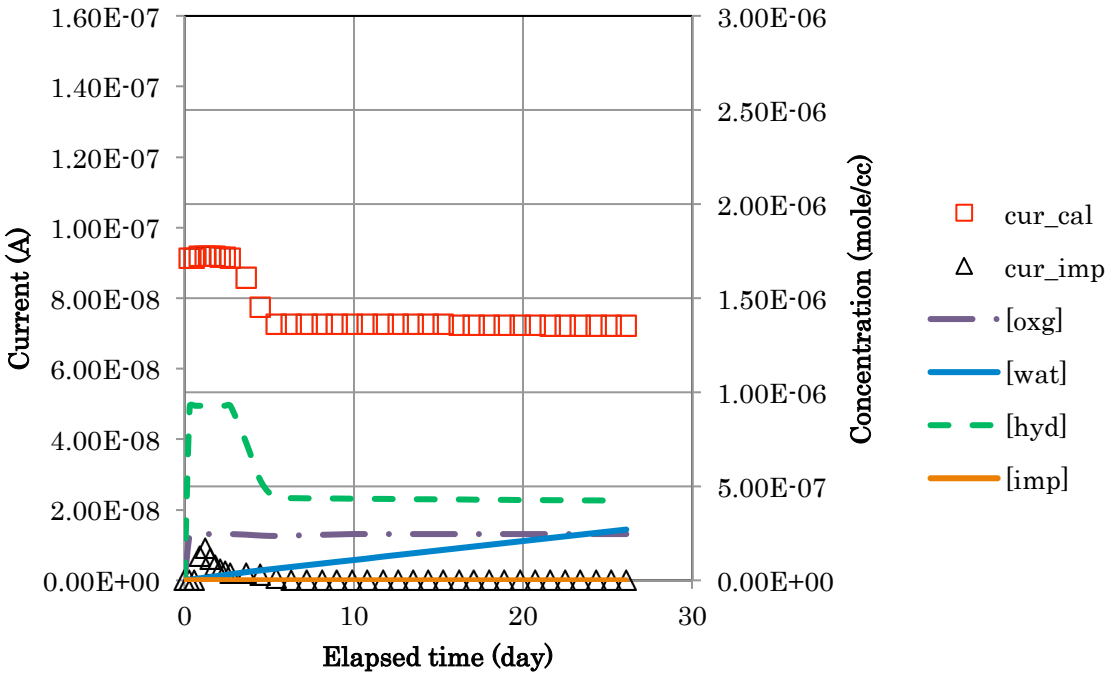

Figure 3.4 Detailed results of calculation current and concentrations for The experiment under reactor neutrino irradiation.

The impurity current and the concentrations of ions are shown in **Fig. 3.4**. The product $P_c[\mathrm{H}^+ v_b]^4[\mathrm{O}_2]$ is again influenced to the output current. The current $I_{\mathrm{H_2O}}$ is considered small in all period in the experiment. Oxygen gas and hydrogen ion concentrations reach the saturation at the first day of the experiment. They decreased quickly after stopping irradiation, due to influence of vibration effect of water during the transportation to Kyushu University. After the transportation, the hydrogen ion concentration is kept still high and decreases dominantly according to eq. (3.10) by the excess recombination to water, while the oxygen gas concentration almost reaches the saturated value. Therefore, the current gradually decreases with elapsed time in Kyushu University.

The fitting procedure of the non-irradiated mixture water and non-irradiated raw silk experiment is similar to the case of environmental and reactors neutrinos. The first peak achieved 60 nA after three days. Then it decreased to 40 nA after four days. Thereafter current started to increase until 140 nA after two weeks. The lower graph of **Fig. 3.5** demonstrates the results of the this experiment. The steep increase of the

output current results from the gradual change of E_{AU}/kT due to accumulated $(Hv_b)_2O$ in the water as

$$E_{AU} / kT = 7.1 \ln \frac{[(Hv_b)_2 O]}{a} b \tag{3.12}$$

with the a and b were set at 6 x 10^{-8} and 0.6, respectively. The calculation graphs are in agreement with experimental data, and the output current reaches a somewhat stable equilibrium.

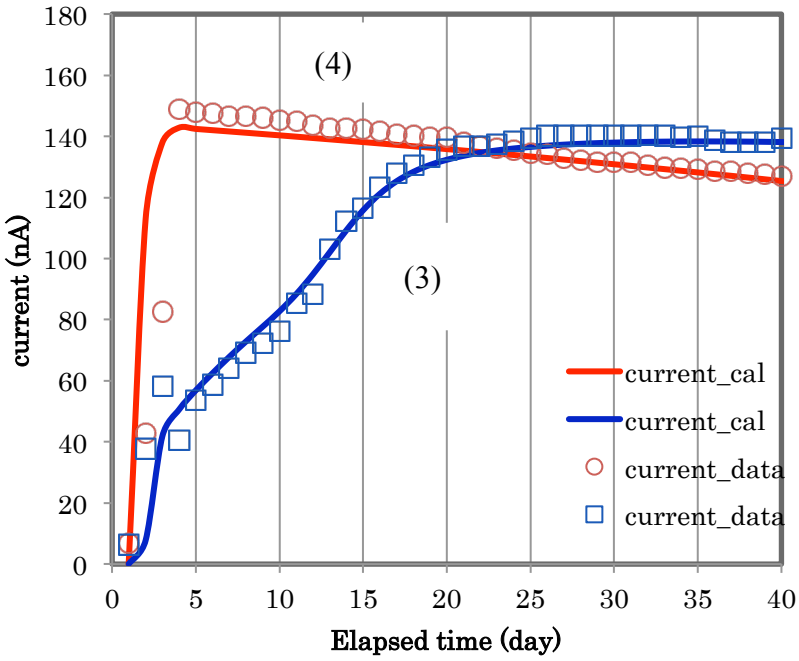

Figure 3.5 Calculated output current versus time. The lower curves are the calculation results for the non irradiated mixture water and non irradiated raw silk experiment. The value of E_{AU}/kT gradually increases from zero to 7.1. The upper curves show the calculation results obtained for irradiated mixture water and irradiated raw silk experiment. The value E_{AU}/kT was constantly 7.1.

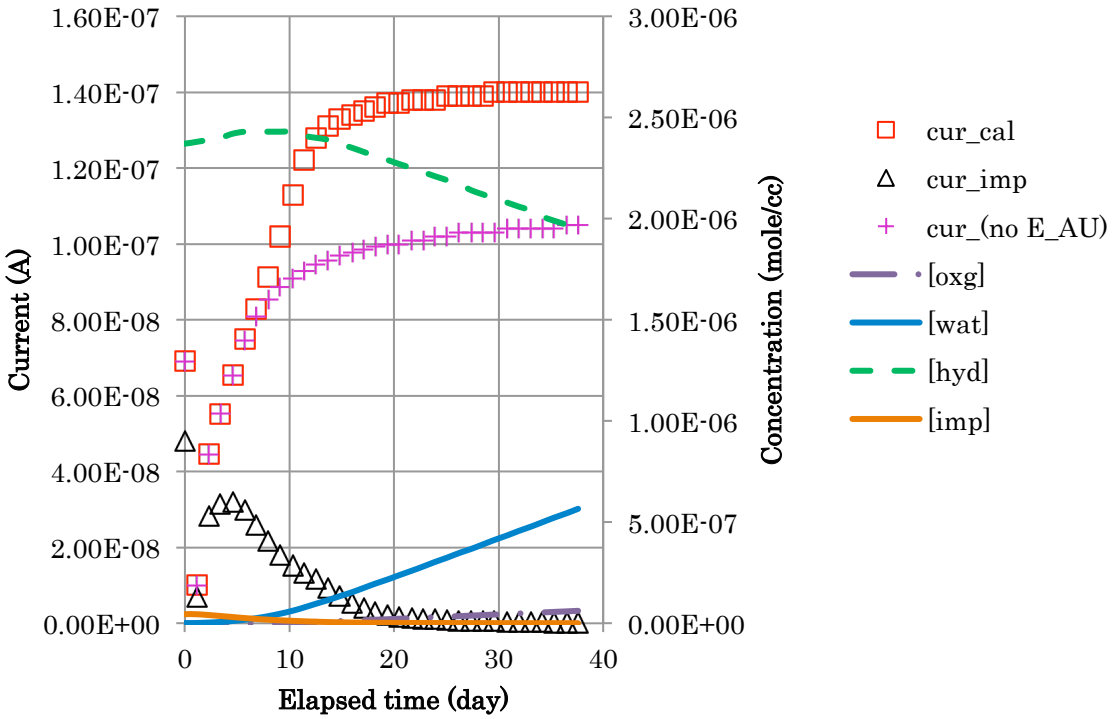

Figure 3.6 Detailed results of calculation current and concentrations for non irradiated mixture water and non irradiated raw silk. The value of E_{AU}/kT was initially set at 0 and increased to 7.1 according to the density $[H^+ \nu_b]$. The cross marks indicate the total current in the case of $E_{AU} = 0$.

The hydrogen ion mostly saturates at 2.4 x 10^{-6} (mol /cc) while oxygen concentration remains at 1.5 x 10^{-7} (mol /cc). Based on eq. (2.6) the hydrogen ion concentration increases gradually because of dissociative ionization reaction between water and neutrino. Hydrogen ions and oxygen molecules are accumulated through the reduction reaction in eq. (2.8) around the carbon electrode. At the same time, the oxidation reaction also occurs in the carbon electrode as in eq.(2.7). The output current increases as the accumulation of hydrogen ion and oxygen in the detector.

The same procedure was also applied to calculate the corresponding solution of hydrogen ion and oxygen concentrations for the irradiated mix-water and irradiated raw silk experiment. The results are given in **Fig. 3.7**. The increase of the output current was ascribed to the higher values of E_{AU}/kT and initial concentration gas, which may be produced by accumulated $[(H^+ \nu_b)_2O]$. The cross marks in the figure

stand for the total current in the case of E_{AU} = 0. The hydrogen ion concentration is saturated at 1.6 x 10^{-6} (mol /cc) at the beginning, and decrease rapidly by the reduction reaction in carbon electrode.

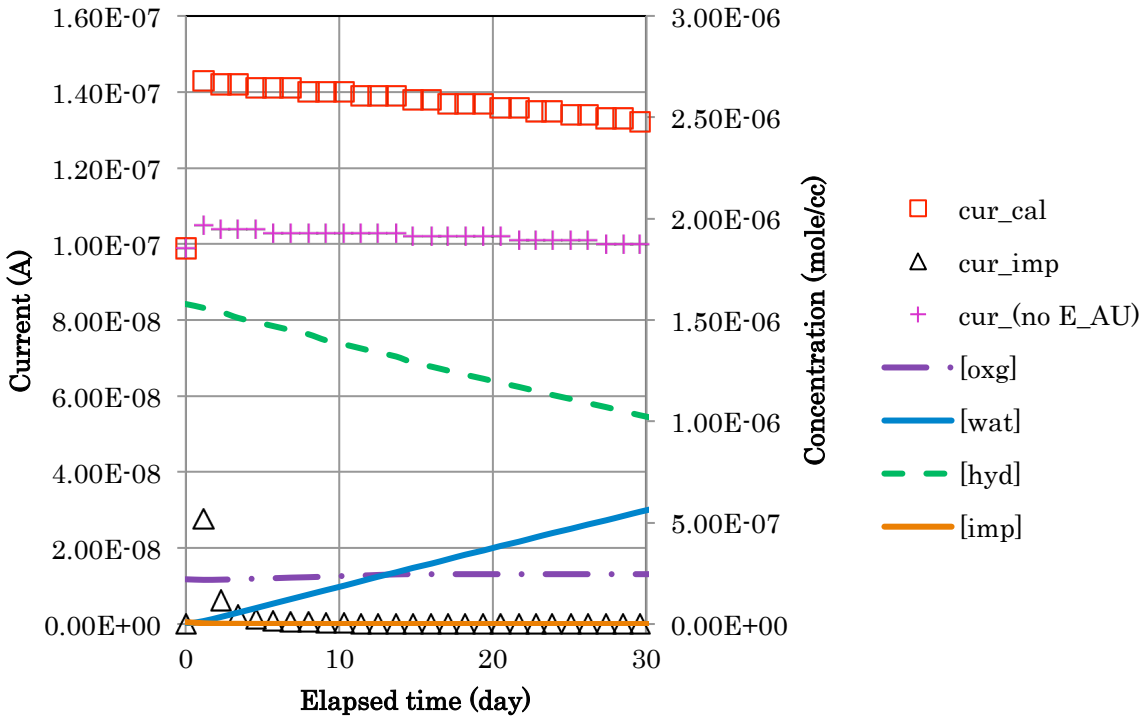

Figure 3.7 Detailed results of calculation current and concentrations for irradiated mixture water and irradiated raw silk. The value of E_{AU}/KT was set at 7.1 in calculation. The cross marks indicate the total current in the case of E_{AU} = 0.

Current output of the fourth experiment is given in **Figs. 3.5** and **3.7**. The experimental data are indicated by circles, while solid line represents calculation one. The curve of this experiment produces a higher current than other experiments. It achieves 150 nA at the beginning. The current decreases only by 25 nA after 38 days. The increasing values should come from the irradiation effect of antielectron neutrinos from the thermal reactor. The irradiation increases the oxygen gas consideration to the saturated density. The effect of E_{AU} is assumed large as inferred from the comparison between the marks of square and cross.

The antielectron neutrino from the thermal reactor contributes to the higher rate of ion concentration. This effect is evident in the second experiment where the hydrogen

ions increase rapidly for two weeks over normal condition, the irradiation process was also contributed in the fourth experiment as increasing current at the first week of experiment. The results of the reactor neutrino experiment suggest the following processes : dissociative ionization of water molecule in eq. (2.6) is more active by 10^4 times in the reactor neutrino irradiation than the natural radiation of environmental antineutrinos in Kyushu University. Thus the hydrogen ion concentration reached the saturation limit at the first day experiment, and decreased gradually after irradiation, this evidence is influenced by vibration effect of the detector when it was transported to Kyushu University. Finally, current decreased by reduction of hydrogen ion concentration while experiment was continued in the laboratory of Kyushu University.

The reaction rate of water dissociative ionization was R_{H_2O} = 2.24 x 10^{-13} mol cm^{-3} s^{-1} for the first experiment under natural condition. The geoneutrino flux is φ_v = 5.7 x 10^5 cm^{-2} s^{-1} in the energy region below 50 keV. The cross section of water dissociation reaction by antineutrino is estimated to be $\sigma \approx 10^{-18}$ cm^2. This value is quite large in comparison with a typical cross section around $\sigma \approx 10^{-40}$ cm^2. It was considered that the compounds $H^+ v_b$ and $e v_f$ are formed under the influence of B^0 and both have dimensions similar to an atomic size. The low energy antielectron neutrino with constituents of weak charge and weak dipole moment is estimated[6] to be in a sparse situation and be in an atomic size. A bound system in the atomic size is considered to have a binding energy comparable to energy of eV, according to a harmonic oscillator model.

We can tell that a simple Born approximation for eq. (2.6) with eV-range interaction energy and atomic size produces the interaction cross section of 10^{-19} cm^2. This quantity is qualitatively in agreement with the cross section from the half-cell model.

Chapter 4 Influences of Solar Wind Velocity

4.1 Solar Wind

The electrochemical apparatus tends to make a peak current at first a few days (we called 'initial peak' thereafter). The initial peak has a large variation in height in individual measurements. As one of possible reasons for the variation, it is interesting to consider the effect of solar activity. The solar activity has a periodicity of 28 days. Among the activity, the solar wind velocity also varies on the same periodicity. The solar wind has a relationship to geomagnetism. The solar wind may affect geomagnetism and the transportation of low-energy geoneutrinos or their fragments. As a result by examining our data of the past half-year, we found a positive correlation between the solar wind velocity and the initial peak current. Therefore, we continue the experiment to study whether the correlation is true or not.

4.2 Experiments

To study the effect of solar wind the experiment was carried out by six electrochemical detectors. The detectors provide six signals to give more reliable tendency under environmental conditions. The experimental apparatuses were placed in the incubator at a temperature of 27 degrees centigrade. The run time was typically 20 days in each period.

As an example, the output voltage of six detectors are shown in **Fig. 4.1**. The wire connection method was changed to employ silver-paste bonding, instead of use of soldering in the previous experiment[58]. This promotes the output voltage almost twice, and produces the value around 100 mV. The standard deviation of voltage signal is 10 % in sigma and three times as large as the previous experiments. The signal growth to the twice magnitude is supposed to be related to the increase of the auxiliary field B^0. The three-fold variation may be ascribed to the fluctuation in B^0 growth in the apparatus.

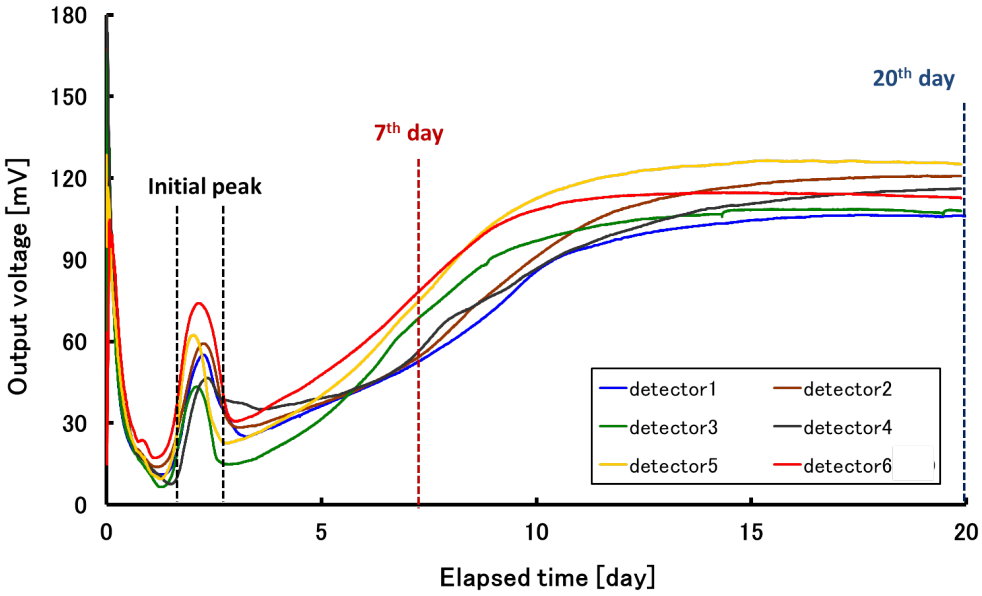

Figure 4.1 Example of output voltage as a function of elapsed time for individual detectors.

4.3 Influence by solar wind and geomagnetic indices

The environmental neutrinos may be influenced by solar activities. The correlation was observed between the output voltage and the solar characteristics data available by an artificial satellite and observatories. The solar wind is a stream of charged particles ejected from the upper atmosphere of the sun with kinetic energies usually between 10 and 100 keV.

We took the Real-Time Solar Wind (RTSW) data from the spacecraft of Advanced Composition Explorer (ACE) which were available by the Space Weather Prediction Center (SWPC) as updating data lists and plots. **Figs. 4-2** to **-5** present the relationship between solar wind velocity and the average output voltage at three different days of elapsed time. Here, the data of solar wind velocity are referred at the instantaneous value corresponding to the time of the initial peak. For the initial peak, the time duration of output voltage reaching the maximum value varies in each measurement, so that, the horizontal error bar is specified only for the initial peak average. For the

data of 7th and 20th days, the time of measurements are uniquely determined as those days. The data of solar wind velocity referred have a small variation for each detector. Thus, the plots of 7th and 20th days have horizontal error bars of a very small range. We classified the data of output signals according to the period in measurement: Data 1 was obtained during No. 2010 ~Feb. 2011, Data 2 Apr. 2011~Jul. 2011, Data 3 Oct. 2011~Jan. 2012 and Data 4 Jan. 2012~Jul. 2012. The numbers appearing in **Figs. 4-2** to **-5** stands for the measurement order in experiments. The dashed line in the figure was drawn by the least-square-fit to the output voltage at the initial peak point. The data at the initial peak tend to show some correlations. For paired data $(x_i,\ y_i)$, the Pearson correlation coefficient r is given by

$$r = \frac{\sum_{i=1}^{n}(x_i-\bar{x})(y_i-\bar{y})}{\sqrt{\sum_{i=1}^{n}(x_i-\bar{x})^2}\sqrt{\sum_{i=1}^{n}(y_i-\bar{y})^2}}\ , \qquad \text{correlation coefficient} \tag{4.1}$$

where $\bar{x}$ and $\bar{y}$ are the sample mean of x_i and y_i, respectively.

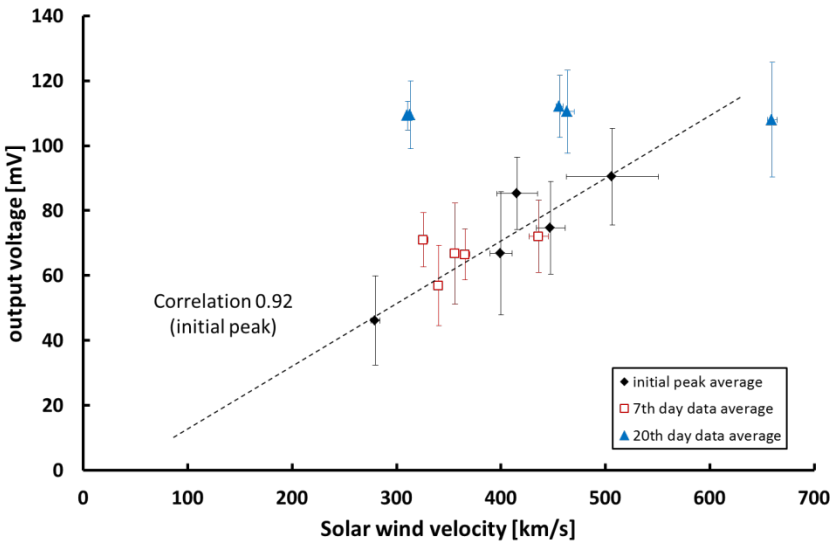

Figure 4.2 Correlation between the output signal and solar wind velocity for Data 1 (Nov. 2010~Feb. 2011).

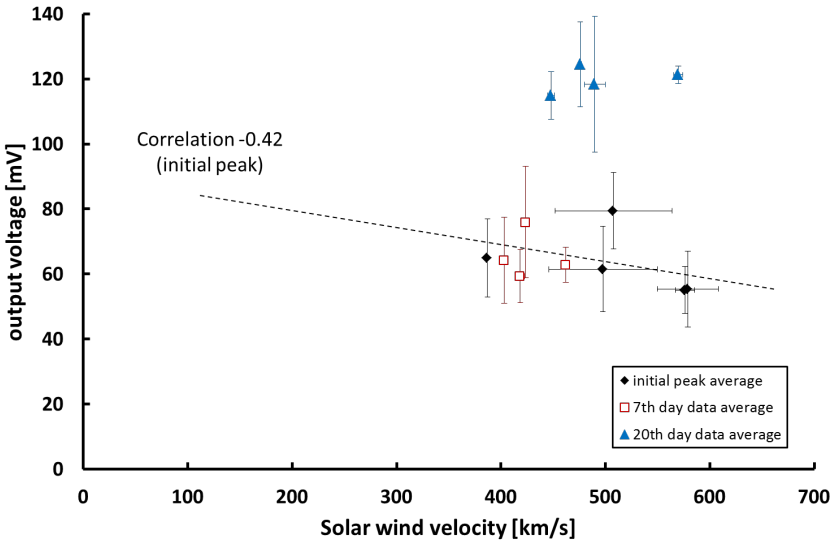

Figure 4.3 Correlation between the output signal and solar wind velocity for Data 2 (Apr. 2011~Jul. 2011).

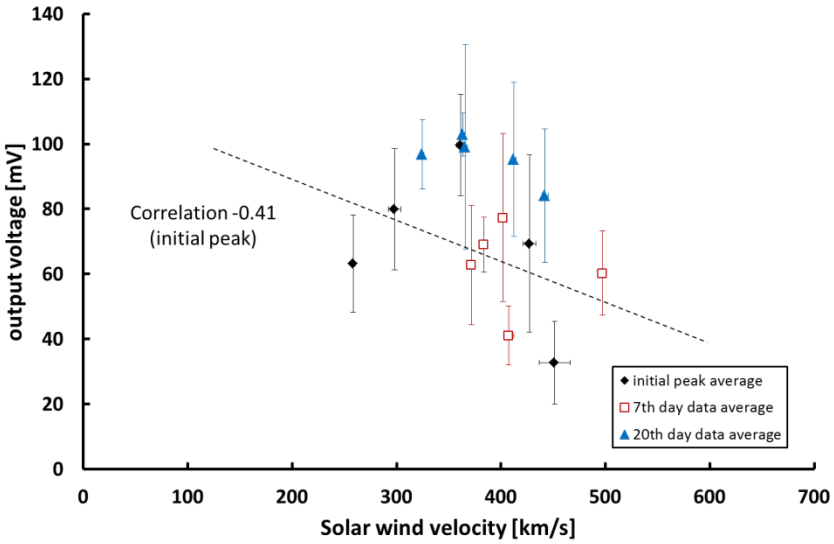

Figure 4.4 Correlation between the output signal and solar wind velocity for Data 3 (Oct. 2011~Jan. 2012).

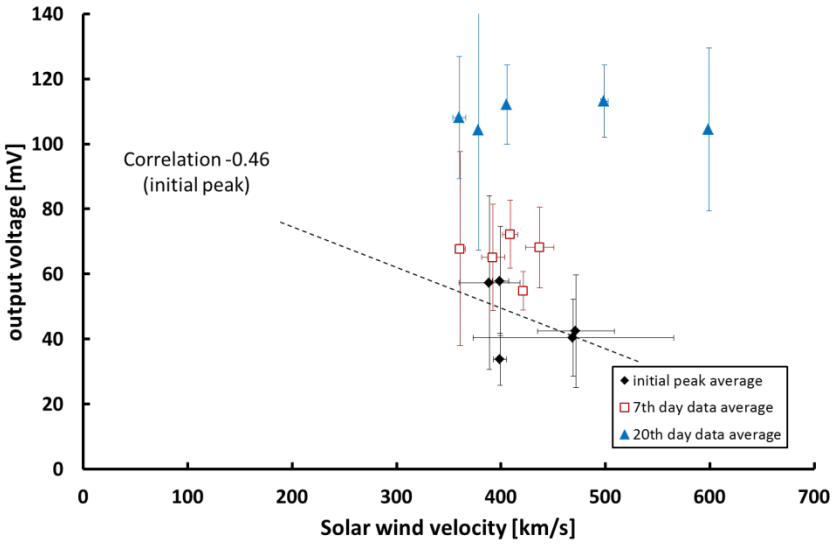

Figure 4.5 Correlation between the output signal and solar wind velocity for Data 4 (Jan. 2012~Jul. 2012).

The dashed line in **Fig. 4.2** exhibits a good correlation (0.92). The correlation provided the motivation of the study in this chapter. However, the others do not show appreciable correlation. These correlation coefficients are summarized in **Table 4.1**, where positive and negative values are scattered. As a whole, there is no tendency to imply the relationship between the solar activity and the output voltage from the solar wind velocity. We recall that the apparatus produced the large experimental signal near the nuclear reactor, where antielectron neutrinos were dominant. The geoneutrinos (antielectron neutrinos) are supposed to be basically independent of the solar activity.

Table 4.1 Correlation coefficients between the output voltage and the solar wind velocity.

	Initial peak	7^{th} day	20^{th} day
Data.1 (Nov.2010~Feb.2011)	0.92	0.44	-0.27
Data.2 (Apr.2011~July.2011)	-0.42	-0.08	0.40
Data.3 (Oct.2011~Jan.2012)	-0.41	-0.16	-0.74
Data.4 (Jan.2012~July.2012)	-0.45	-0.20	-0.12

Chapter 5 Conclusion

In this study, the half-cell model with assistance of weak interaction was studies for numerical calculation of the output current of the apparatus, and the reason was experimentally investigated for poor reproduction of the initial peak in the output current behavior.

For electrochemical apparatuses, four types of measured results were adopted as described in Chapter 2. The first experiment was the measurement under environmental conditions, and the second was that under nuclear reactor neutrino irradiation. The third experiment used both the water from raw-silk soaked solution and a fresh raw silk, while the fourth utilized those under nuclear reactor neutrino irradiation. The effect of the nuclear reactor neutrino irradiation was appreciably larger on the output currents in the second and fourth experiments. To understand the experimental signal behavior, a scenario was proposed of output current generation: A neutrino is composed of boson and fermion constituents. When neutrinos are incident into auxiliary field generated from the biological material, they will obtain larger mass and tend to separate into boson and fermion particles. The neutrinos may also induce water molecule to make dissociative ionization into hydrogen and hydroxide ions. The hydrogen ion H^+ combines with the boson particle while the hydroxide one OH^- does with fermion. The repulsive properties of boson and fermion constituents at rest do not allow the ions to be recombined. The hydroxide ions with fermion may diffuse to a gold plate, whereas hydrogen ions with boson may move to a carbon one. The electrochemical reaction at the electrodes was assumed to take place for generation of the output current.

For numerical analysis of output current calculation, a half-cell model with assistance of weak interaction was presented in Chapter 3. The time evolution of output current was solved with the half-cell model. The current density of hydrogen ions was given by the Butler-Volmer equation as the reduction reaction by oxygen gas. The activation energy in the equation was obtained from experimental data at different temperatures as $\Delta = 0.65$ eV. The reaction of hydroxide ions is endothermic one; the reaction was assumed to be promoted with assistance of weak interaction between the fermion particle and the auxiliary field. The hydrogen ions were treated

to disappear in the rate of I/F as the current I flows where F is the Faraday constant. The oxygen gas was postulated to be produced by the neutrino reaction. For reproduction of experimental current, however, time parameters t_d and t_r were adopted for expressing the delay and rising times, respectively, for initiation of weak interaction assistance. The values of t_d and t_r of few days were treated as adjustable parameters.

The comparison between the experiments and calculations suggested that the half-cell model works well for the environmental experiment. The same electrochemical parameters were applied to the experiments under reactor-neutrino irradiation conditions. When an estimated reactor neutrino flux was adopted, the output current was twice as large as the experiment, but the larger signal was successfully suppressed by setting limited value of hydrogen ion concentration. Thus, the use of basically the same electrochemical parameter leads to reproduction of the experimental data. For other experiments based on the water from raw-silk soaked solution and a fresh raw silk, an assumption was additionally made on the other cell as the voltage between the gold electrode and the solution. This additional voltage was required for reproduction of the experimental data. From these calculation results, the effect of reactor neutrino irradiation was confirmed to exist on the output currents in quantitative manner.

The poor-reproductive characteristics of initial peak were experimentally studied in Chapter 4. The output current of electrochemical apparatus under environmental conditions gives an initial peak around 2 days and an equilibrium value in 2-3 weeks under environmental conditions. At early stage of our experimental study, a tendency of positive correlation was observed between the initial peak and solar activity, namely, solar wind velocity. To make clear the situation, further experiments were carried out during the period for one year. For the later experiments, some tendency was seen, but no clear correlation was found throughout whole experiments. It was concluded that the former positive correlation in the early stage was the accidental result.

Future prospects of this study are as follows,

1. It is required to improve the more realistic formulation of oxygen generation, instead of use of constant fraction in the neutrino reaction rate.
2. It is necessary to make the experiment to measure hydrogen in addition to oxygen gas.
3. In the new experiments under reactor neutrino irradiation experimental detectors need to be located at different positions from the reactor core to clarify the effect of distance on the output signal.

REFFERENCES

1) L. M. Brown, The idea of the Neutrino, Physics Today **31**(9), 23(1978).

2) C.D. Ellis, W.A.Wooster, The average Energy of Disintegration of Radiation E, Proceedings of Royal Society A **117**, 109 (1927).

3) N. Bohr, Faraday Lecture, J. Chem. Soc. 349 (1932).

4) E. Fermi, Versuch einer Theorie of der beta-StrachlenI, Z. Phys. **88**, 161 (1934).

5) K. C. Wang, A Suggestion on the Detection of the Neutrino, Phys. Rev. **61**, 97 (1942).

6) C. L. Cowan, Jr., F. Reines, F.B. Harrison, H. W. Kruse and A. D. McGuire, Detection of the Free Neutrino: a Confirmation, Science **124**, 103 (1956).

7) C. M. G. Lattes, H. Muirhead, G. P. S. Occhiailni and C. F. Powell, Processes involving Charged Mesons, Nature **159** (4049), 694 (1947).

8) G. Danby, J-M. Gaillard and Goulianos, L.M. Gaulianos, N. Mistry, M. Schwartz and J. Stein berger, observation of high-energy Neutrinos, Phys. Rev. Letter. **9**, 36(1962).

9) K. Kodama, et. Al., Observation of Tau Neutrino Interactions, Phys. Letter. B **504**, 218 (2001).

10) D.H. Perkins, Introduction to High Energy Physics, Addison-Wesley(1987).

11) L. Wolfenstein, Neutrino Physics, Rev. Mod. Phys. **71**, 2 (1999).

12) Neutrino Experiment, Nuclear Fission and Fussion, and Nuclear Interactions, NLP National Physical Laboratory. 2008.

13) F. Reines, C-Cowan Jr., The Reines – Cowan Experiments: Detecting the

Poltergeist, Los Alamos Science **25**,3,1997.

14) A. Bernstein, et al; Wang, Y, : Gratta, G: West, T. (2002), Nuclear Reactor Safe Guards and Monitoring with Antineutrino detectors, Journal of Applied Physics **991**(7) : 4672.

15) Bandyopadhyay et al. (ISS Physics Working Group), Physics at Future Neutrino Factory and Super-beam Facility, Reports on Progress in Physics **72**(10): 6201.

16) Frank. T. Avignone III, Steven R. Elliott, Double Beta Decay, Majorana Neutrinos, and Neutrino Mass, Rev. Mod. Phy. **80**. 481 (2008).

17) J. Bahcall et. Al., Serenelli, New Solar Opacities, Abundances, Helioseismology, and Neutrino fluxes, The Astrophysical Journal **621**: L 85-L88. (2005).

18) R. M. Bionta, et. Al., Observation of a Neutrino Burst from the Supernova SN 1987 A, in the Large Magellanic Cloud, Phys. Rev. Letter.

19) J. N. Bachall, H. M. Pinsonnealt, Solar Model: Current Epoch and Time Dependences, Neutrinos, and Helio seismological Properties, Astrophys. J. **555**, 990 (2001).

20) S. A. Colgate, R.H. White, The Hydrodynamic Behaviour of Supernova Explosions, The Astrophysical Journal **143**: 625, 1996.

21) J. Bahcall et. Al., Serenelli, New Solar Opacities, Abundances, Helioseismology, and Neutrino fluxes, The Astrophysical Journal **621**: L 85-L88. (2005).

22) R. M. Bionta, et. Al., Observation of a Neutrino Burst from the Supernova SN 1987 A, in the Large Magellanic Cloud, Phys. Rev. Letter.

23) A. K. Mann, Shadow of A Star, The Neutrino Story Story of Supernova 1897A. W.H. Freeman. P. 122, 1997.

24) S. Eldeman, et al., Review of Particle Physics, Phys. Lett. B **592**, 1(2004).

25) Borexino Experiment, Gran Sasso, 2011.

26) Georg.G. Raffelt, Borexino, Stars As Laboratories for Fundamental Physics: The Astrophysics of Neutrinos Univ. of Chicago Press. Pp. 393-394, 1996.

27) Borexino Collaboration, Measurement of CNGS. Muon Neutrino Speed with Borexino, Physics Lett. B **716** (3-5) 401 – 405, 2012.

28) Borexino Collaboration, Succeeds inspotting pep Neutrinos Emitted from the Sun, Physorg. Com, 2012.

29) Emiliano Feresin , Low-energy Neutrinos Spotted, Nature News, 2007.

30) Gallex Collaboration, Gallex Solar Neutrino Observations : Complex results for GALLEX II, Physics Letters B, **357**, 237 (1995).

31) Martin, B. R, et al., Particle Physics (2^{nd} edition). Willey. P. 265, 1999.

32) A. T. Cleveland, et al., Measurement of the Solar Electron Neutrino Flux with the Homestake Chlorine Detector, Astrophysical Journals **496**: 505 – 526, 1998.

33) K. Lande, in Talk at Neutrino 98 Takayama, ed. (1998).

34) John N. Bachall, Sarbani Basu, and M. H. Pinsonnealt, How Uncertain are Solar Neutrino Prediction, Physics letters B, **433**, 1(1998).

35) A. Iversion, The measured resistivity of Pure Water and Determination of the Limitting Mobility of OH^- from 5 to 55^0, The Journal of Physical Chemistry, **68**, 515 (1964).

36) Yong-Woo Lee, Silk Reeling and Testing Manual, FAO Agricultural Services Bulletin, No. **136** (1999).

37) R.S. Nicholson, Theory and Application on Cyclic Voltammery for

Measurement of Electrod Reaction Kinetics, Analytical Chemistry, **37**, 1351 (1965).

38) S. Yamada and Sato, Some Physical Properties of Glassy Carbon, Nature, **193**, 261(1962).

39) B.l E. Conway, H. Angerstein, et al., Analytical Chemistry, **45**, 1331 (1973).

40) R. N. Adams, Electrochemistry at Solid Electrodes, Marcel Dekker, New York, 1969.

41) J. O. M. Bockris and A. K. N. Reddy, Modern Electrochemistry, vol. 2, Plenum Press, New York, **1156** (1970).

42) S. Trassatti, Work Function Electro gravity and Electrochemical behavior of Metals, III. Electrolytic Hydrogen Evolution in Acid Solution, Journal of Electro analytical Chemistry, **39**, 163 (1972).

43) P. W. At kins, Physical Chemistry, Oxford University Press. (1998).

44) T. Nishimura, Study on Neutrino Flux from Nuclear Reactor and Neutrino Structure, Doctoral Dissertation, Kyushu University (2008), [in Japanese].

45) S. Enomoto, http://www.awa.tohoku.ac.jp/~sanshiro/research/geoneutrino/spectrum/ index.html.

46) Davies, J. H., Davies, D. R. Earth's surface heat flux. *Solid Earth* **1** (1): 5–24, 2010.

47) Liu Wei, K. Ishibashi, et al., *J. Nucl. Sci. Technol.*, *Suppl.*, **4**, 487-490 (2004).

48) A. Lautrup, K. Dan. *Vidensk.Selck.Mat.-Pys.Medd.* **35**, 11 (1968).

49) Hershenhart, R. L. McCreery and R. D. Knisht, Insitu Cleaning and Activation of Solid Electrode Surfaces by Pulsed Laser Light, Analytical Chemistry, **56**, 2256 (1984).

50) K. Ishibashi, N. Terao, et al., *Prog. Nucl. Sci. Technol.*, **1**, p.348-351 (2011).

51) J.H. Hirschenhofer, D.B. Stauffer, et al., *Fuel Cell Handb*ook, Parsons Corp., Reading PA (1998).

52) K. Ishibashi, Liu Wei, et al., *Prog. Nucl. Sci. Technol.*, **1**, p.436-439 (2011).

53) Liu Wei, Study on Detection of Environmental Neutrinos by Means of Miniaturized Apparatuse Based on Electrochemical Reaction, Doctoral dissertation, Kyushu University (2004).

54) A. J. Bard, L.R. Faulkner, Electrochemical methods, Fundamentals and Applications, John Wiley & Sons, New York (2001).

55) C. Quigg, "Gauge Theories of the Strong, Weak and Electroweak Interactions," (Boulder, CO:Westview, 1998), D.H. Perkins, "Introductions to High Energy Physics," (Menlo Park, CA: Addison-Wesley, 1988).

56) Akasofu, P.Perreault, S.-1. Akasofu, A Study of Geomagnetic Storms, Geophys. J. R. Astro. Soc. **54**, 547-573 (1998).

57) J.N. Abdurashitov, et al., *Phys. Rev. C* **60** 558011-5580132 (1999).

58) G. Kallen, *Quantum Electrodynnamics,* Springer-Verlag, Berlin (1972).

59) N. Nakanishi, *Prog.Theor.Phys.* **35**, 1111 (1967); *Prog. Theor. Phys.* **38**, 881 (1968).

60) M. Modal, K. Trivedy, et al., 'The Silk Proteins, Sericin and Fibroin in Silkworm, Bombyx mori Linn.', Caspian J. of Env. Sci. Vol. 5, **2**, P. 63-76, 2007.

Acknowledgements

This study has been carried out at the Department of Applied Quantum Physics and Nuclear Engineering, Graduate School of Engineering, Kyushu University, under the supervision of Professor Kenji Ishibashi. This dissertation would not have been possible to be completed without the help and support of many people who are grateful acknowledged here

First of all, I would like to express my deepest gratitude to my supervisor, Professor Kenji Ishibashi, with whose teaches and supports I could complete my research works and the dissertation. He has given me patient guidance, encouragement and supports throughout the period of my doctoral course at Kyushu University. I greatly appreciate that, by working with him, I improved not only my knowledge, of physics and scientific writing, but also the rigorous attitude in scientific research work. The things which I learnt from him are of great value to me, and will surely be important for my future works.

I would like to express my sincere appreciation to Prof. Nobuo Ikeda, Department of Applied Quantum Physics and Nuclear Engineering, Graduate School of Engineering and Prof. Satoshi Fukada, Department of Advanced Energy Engineering Science, Interdisciplinary Graduate School of Engineering Sciences, for their encouragement, carefully reading of this manuscript and valuable comments.

My deeply thanks to Associate Professor Keisuke Maehata, Associate Professor Naoko Iyomoto and Assistant Professor Nobuhiro Shigyo for their warmhearted concern and friendly help in the Ishibashi laboratory.

Furthermore, I would like to thanks to Prof. Zaki Su'ud, Department of Physics, Bandung Institute of Technology, who introduced me to nuclear science.

My heartfully appreciate to neutrino group, Norichika Terao, Shouhei Nakamura, Youichi Imahayashi, and Shoya Suda for any discussion and learning together, and to Liu Wei for providing the experimental data.

Special thanks to the Ishibashi Laboratory members for their kindness in Laboratory. My special thanks also to my tutor Yasumune-san, Maida-san. Kajimoto-san, Halim-san and Hao-san.

Deeply thanks is also given to Ms. Yasura Oiwa for help in her office work.

The scientific and financial support from Kyushu University and Japanese Ministry of Education, Culture, Sports, Science and Technology under the MONBUKAGAKUSHO Scholarship is gratefully acknowledged.

At last but not least, I am grateful to my husband, my family, lovely Kids Aurora Muthmainnah and Hafaz Ahmad Zaki.